Protein Control of Redox Potentials of Iron–Sulfur Proteins

P. J. Stephens,* D. R. Jollie, and A. Warshel

Department of Chemistry, University of Southern California, Los Angeles, California 90089-0482

Received March 18, 1996 (Revised Manuscript Received July 1, 1996)

Contents

I. Introduction

Iron−sulfur ([Fe-S]) proteins[1−3] contain iron−sulfur ([Fe-S]) clusters in which iron atoms are wholly or predominantly coordinated by sulfur atoms. The sulfur atoms are of two types: cysteine S_γ and monatomic, "inorganic" S.

The simplest [Fe-S] clusters are those in which Fe is the only metal present and all Fe atoms are wholly ligated by S. Examples are the 1Fe, 2Fe, 3Fe, and 4Fe clusters whose stoichiometries are:

1Fe	$FeCys_4$	2Fe	$Fe_2S^*_2Cys_4$
3Fe	$Fe_3S^*_4Cys_3$	4Fe	$Fe_4S^*_4Cys_4$

where S* denotes inorganic sulfur. The 3D structures of these clusters are shown in Figure 1. Fe is four coordinate, each cysteine S_γ ligates one Fe and inorganic S bridges multiple Fe atoms. Clusters are also known in which other metals, in addition to Fe, and/or other ligands, in addition to cysteine, are present.

[Fe-S] clusters exhibit reversible oxidation−reduction between different oxidation levels. Oxidation levels can be defined by the total cluster charge and by the formal oxidation levels of the Fe atoms obtained assuming cysteine and inorganic sulfur to have charges of −1 and −2, respectively. In the simple 1Fe, 2Fe, 3Fe, and 4Fe clusters, the following redox couples are well known:

	cluster charges	formal Fe oxidation levels
$FeCys_4$	1−/2−	Fe^{3+}/Fe^{2+}
$Fe_2S^*_2Cys_4$	2−/3−	$Fe_2{}^{3+}/Fe^{3+},Fe^{2+}$
$Fe_3S^*_4Cys_3$	2−/3−	$Fe_3{}^{3+}/Fe_2{}^{3+},Fe^{2+}$
$Fe_4S^*_4Cys_4$	2−/3−	$Fe_2{}^{3+},Fe_2{}^{2+}/Fe^{3+},Fe_3{}^{2+}$
	1−/2−	$Fe_3{}^{3+},Fe^{2+}/Fe_2{}^{3+},Fe_2{}^{2+}$

The redox potentials of [Fe-S] clusters in [Fe-S] proteins vary widely,[4] the most positive being >+400 mV (vs SHE) while the most negative are <−600 mV.

For many [Fe-S] proteins, the redox potentials of their [Fe-S] clusters are of physiological importance. While the functions of many [Fe-S] proteins are not firmly defined, it is widely believed that the large majority are electron transport proteins. The kinetics of electron transfer between proteins is a sensitive function of their relative redox potentials.[5] For those [Fe-S] proteins engaged in electron transport, the redox potentials of their clusters are thus of central importance to their biological function.

In this article we discuss the relationship between the structure of an [Fe-S] protein and its redox potential. Specifically, we address the question: for a given [Fe-S] cluster, what are the origins of the variations in redox potential exhibited by different proteins? This question has been debated extensively in the literature. Evidence has been adduced for the importance of a variety of parameters, such as cluster−protein hydrogen bonding, cluster solvent accessibility, and the number of charged residues. Here, we describe a new approach to understanding the protein control of [Fe-S] cluster redox potentials: quantitative modeling. Molecular modeling is increasingly widely used in predicting and understanding the energetics of biological molecules and their chemical reactions.[6,7] Here, we discuss the application of this general methodology to the specific problem of redox potentials. We present and discuss the results of recent studies[8−10] of the redox potentials of [Fe-S] proteins carried out using the microscopic methodology developed by Warshel and co-workers and referred to as the Protein Dipoles Langevin Dipoles (PDLD) model.[11,12] The protein is modeled as a collection of charged, polarizable atoms. Aqueous solvent molecules are modeled as orientable point dipoles ("Langevin dipoles"). The interaction of the [Fe-S] cluster with the surrounding protein and solvent is evaluated using classical electrostatics. As we will show, this model provides a physically realistic basis for the estimation of the effects of the protein and solvent environments of an [Fe-S] cluster on its redox potential.

S0009-2665(95)00045-8 CCC: $25.00

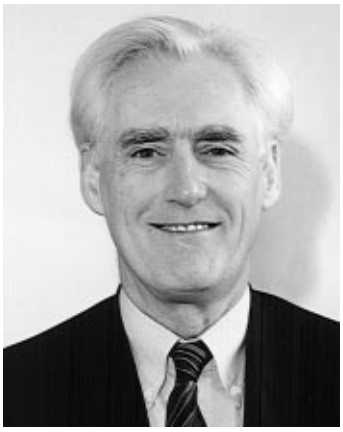

Philip Stephens is a Professor of Chemistry at the University of Southern California and, since 1992, Chair of the Department of Chemistry. He was born in England and educated at Oxford University, receiving B.A. and D.Phil. degrees in Chemistry in 1962 and 1964, respectively. He carried out postdoctoral research at the University of Copenhagen (1964–1965) and the University of Chicago (1965–1967) and then joined the faculty of the Department of Chemistry at USC. His research has been predominantly in the areas of theoretical chemistry, molecular spectroscopy, and bioinorganic chemistry. He is particularly known for his pioneering work, both theoretical and experimental, in the fields of magnetic circular dichroism spectroscopy and vibrational circular dichroism spectroscopy. He is a recipient of an Alfred P. Sloan Fellowship, the USC Associates Award for Creative Scholarship and Research, and a Guggenheim Fellowship.

David Jollie was born in Crystal Lake, IL. He received his B.S. degree in Biochemistry from the University of Illinois at Urbana—Champaign in 1982. He was a research assistant for two years each in the Pharmacology Department at the University of Illinois Health Science Center in Chicago and in the Biochemistry Department at the University of Illinois at Urbana—Champaign. After completing his Ph.D. in Biochemistry at the University of Minnesota, MN, under the tutelage of Professor John Lipscomb in 1992, he took up a postdoctoral position with Professor Philip Stephens in the Department of Chemistry at the University of Southern California. Currently he is an Assistant Professor in the Department of Chemistry and Biochemistry at the University of Maryland in College Park where he is undertaking mechanistic studies of metalloenzymes.

To begin with, we describe the PDLD methodology and summarize the results of PDLD calculations on a range of natural [Fe-S] proteins whose structures have been determined by X-ray crystallography. Next, we evaluate the consequences of molecular dynamics (MD) averaging of PDLD calculations. PDLD and MD-PDLD calculations for a set of mutants of one specific [Fe-S] protein are then compared to experiment. Subsequently, we discuss the contributions of charged residues to redox potentials.

Arieh Warshel is a Professor of Chemistry and Biochemistry at the University of Southern California. He was born in Kibutz Sdhe Nahum, Israel. He received a B.Sc. degree from the Technion Institute in 1966, and M.Sc. and Ph.D. degrees in 1967 and 1969, respectively, from the Weizmann Institute. In his Ph.D. work he developed the Cartesian consistent force field method which is the basis of many current macromolecular simulation programs. From 1970 to 1972, he was a postdoctoral associate at Harvard University. From 1972 to 1976, he was senior scientist and associate professor at the Weizmann Institute during which time he was also an EMBO fellow at the MRC in Cambridge, England. In 1976, he joined the faculty of the Department of Chemistry at USC. Professor Warshel has pioneered computer-modeling approaches to the study of protein function. These include the development of consistent treatments of electrostatic energies in proteins, quantum/classical methods for studies of the energies of enzymatic reactions and the introduction of molecular dynamics simulations to studies of biological processes (in a study of the primary event in the visual process). Professor Warshel is the author of *Computer Modelling of Chemical Reactions in Enzymes and Solutions*, published in 1991. He is a recipient of an Alfred P. Sloan Fellowship and an EMBO Senior Fellowship, the USC Associates Award for Creative Scholarship and Research and the International Society for Quantum Biology and Pharmacology Award for contributions to quantum biology.

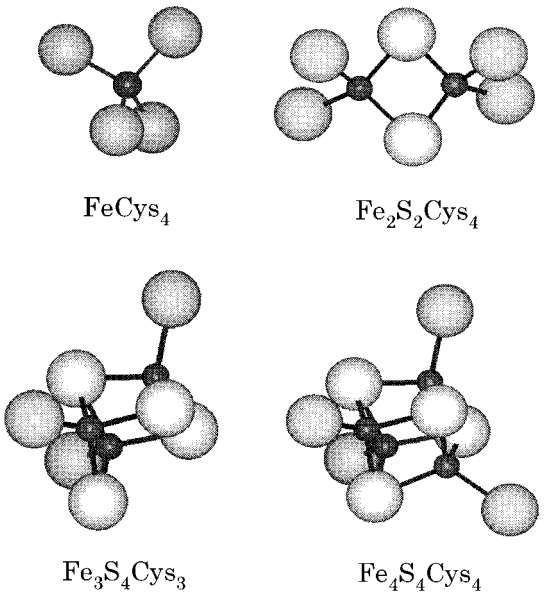

Figure 1. Structures of common iron−sulfur clusters. Iron is represented by the small dark spheres; inorganic sulfide, by the large white spheres; Cys Sγ, by the large gray spheres.

There follow predictions for two specific proteins whose structures are known but whose redox potentials have not been reported. Thereafter, we briefly critique prior discussions of [Fe-S] protein redox potentials and offer a few concluding comments.

II. Modeling Redox Potentials Using the PDLD Approach

The calculation of the redox potential of a redox-active prosthetic group within a protein is the calculation of the difference in the free energies of the oxidized and reduced states. The free energy of a given state is the sum of the intrinsic free energy of the prosthetic group and the free energy of interaction with the surroundings—in this case, protein and solvent. Our goal is to calculate the second of these two contributions, using classical electrostatics. Variations in the protein surrounding the prosthetic group will lead to variations in its free energy—and, hence, in the free energy difference for oxidized and reduced states and the redox potential. If we can successfully model the interaction of a prosthetic group with its environment we can therefore predict the variations of its redox potential with protein. We do not aspire to calculate the intrinsic free energy of the prosthetic group, which requires quantum mechanical calculations.[13] As a result, we cannot predict absolute redox potentials.

The protein and the solvent are both important contributors to the free energy of a prosthetic group and its change with oxidation level. It is therefore important that, in addition to an accurate description of the protein, the solvent is reliably modeled. The solvent model can be microscopic or macroscopic, i.e. individual solvent molecules can be modeled or the solvent can be treated as a continuum dielectric. The former is clearly preferable, while enormously more complex computationally. The PDLD model adopts a microscopic solvent model. At the same time, the solvent molecules are represented by point dipoles and the solvent model is therefore not fully atomic. This compromise is adopted in the interests of computational efficiency.

The PDLD methodology has been used extensively and applied to a range of problems of bioenergetics.[14] Detailed discussions of the PDLD equations and their implementation in the POLARIS program have been presented repeatedly.[11,12,14−18] The first application of the PDLD method to the problem of protein redox potentials was the 1986 study of cytochrome *c* by Churg and Warshel.[15] This work was subsequently extended to a mutant (N52I) of cytochrome *c*.[19] Blue copper proteins have also been studied.[20]

We now discuss the PDLD methodology in more detail and specifically for the case of [Fe-S] clusters of proteins in aqueous solution. We then present the numerical results of calculations on five sets of [Fe-S] proteins, each set containing the same [Fe-S] cluster expressing the same redox couple.

A. The PDLD Methodology

1. Overview

The PDLD method addresses the problem of a protein containing a redox-active prosthetic group—here, an [Fe-S] cluster—embedded in aqueous solvent. The atoms of the [Fe-S] cluster are given charges. The sum of these atomic charges is the net cluster charge. The individual and net charges of the cluster change with cluster oxidation state. The atoms of the protein surrounding the [Fe-S] cluster are given charges and polarizabilities. The sum of these charges is zero, i.e., the total charge equals the cluster charge.

Aqueous solvent is represented as follows: a sphere of radius r_L is defined with the prosthetic group at its center. Water outside this sphere is represented as a continuum dielectric. Water molecules inside the sphere are represented by point dipoles. The sphere is filled by a 3D grid, spacing *s*. Dipoles are placed at all grid points except those for which the distance to a protein atom is $\leq r_A + r_W$ where r_A is the protein atom van der Waals radius and r_W is the water dipole van der Waals radius. That is, water dipoles are excluded when they are too close to one or more protein atoms.

The protein and solvent environment of the [Fe-S] cluster interact electrostatically with the cluster. The interactions are (1) the interaction of the [Fe-S] cluster atom charges with the surrounding protein atom charges; (2) the interaction of the [Fe-S] cluster atom charges with the dipoles induced in the polarizable protein atoms by both [Fe-S] cluster and protein atom charges; (3) the interaction of the [Fe-S] cluster atom charges with the water dipoles; the orientation of each individual dipole is determined by the net electrostatic field of the [Fe-S] cluster atom charges, the protein atom charges and induced dipoles, and all other water dipoles; (4) the interaction of the [Fe-S] cluster atom charges with the aqueous continuum dielectric. Interactions 1, 2, 3, and 4 are referred to as $v_{Q\mu}$, $v_{Q\alpha}$, v_L, and v_B respectively. The total electrostatic interaction of the cluster with its environment is then

$$v = v_{Q\mu} + v_{Q\alpha} + v_L + v_B \quad (1)$$

The interactions are a function of the cluster charge i.e., its oxidation level.

The redox free energy, ΔG, is expressed as the sum of the intrinsic redox free energy of the cluster, ΔG_i, and the contribution of the cluster environment, ΔG_e:

$$\Delta G = \Delta G_i + \Delta G_e \quad (2)$$

In the PDLD model, ΔG_e is approximated by the change in the electrostatic interaction of the cluster with its environment associated with the change in oxidation state, Δv:

$$\Delta v = \Delta v_{Q\mu} + \Delta v_{Q\alpha} + \Delta v_L + \Delta v_B \quad (3)$$

For proteins containing a given [Fe-S] cluster type and redox couple it is further assumed that ΔG_i is a constant. The difference in redox free energy for two proteins, A and B, is then determined entirely by the change in $\Delta G_e = \Delta v$:

$$\Delta\Delta G \equiv \Delta G^B - \Delta G^A = \Delta G_e^B - \Delta G_e^A = \Delta v^B - \Delta v^A \equiv \Delta\Delta v \quad (4)$$

The PDLD model thus permits the *variation* in redox free energy among proteins expressing the same cluster and redox couple to be calculated.[21]

2. Equations

The equations of the PDLD model have been discussed in detail previously;[11,12,14−18] here, we provide a concise summary.

The interactions of the Fe-S cluster and the atoms of the protein, $v_{Q\mu}$ and $v_{Q\alpha}$, are given by

$$v_{Q\mu} = \sum_{i,j} Q_i q_j / r_{ij} \tag{5}$$

$$v_{Q\alpha} = -{}^1/_2 \sum_j \boldsymbol{\mu}_j \cdot \boldsymbol{E}_j \tag{6}$$

where i and j run over cluster and protein atoms respectively, Q_i and q_j are the charges of atoms i and j, separated by r_{ij}, $\boldsymbol{\mu}_j$ is the induced dipole moment of atom j, and $\mathbf{E}_j$ is the electric field at atom j due to the cluster and protein charges. The induced dipole moment $\boldsymbol{\mu}_j$ is given by

$$\boldsymbol{\mu}_j = \alpha_j \mathbf{E}'_j \tag{7}$$

where α_j is the polarizability of atom j and $\mathbf{E}'_j$ is the sum of $\mathbf{E}_j$ and the fields of the induced dipoles of all other protein atoms.

The interaction of the cluster and the water dipoles, v_L, is given by

$$v_L = -{}^1/_2 \sum_k \boldsymbol{\mu}_k^L \cdot \mathbf{E}_k \tag{8}$$

where $\boldsymbol{\mu}_k^L$ is the average dipole moment of the kth water dipole and $\mathbf{E}_k$ is the electric field at dipole k due to the cluster and protein charges. The so-called "Langevin dipole" $\boldsymbol{\mu}_k^L$ is given by the equation

$$\boldsymbol{\mu}_k^L = \mathbf{e}'_k \mu_0 [\coth \chi_k - 1/\chi_k] \tag{9}$$

$$\chi_k = \mu_0 |E'_k| / kT \tag{10}$$

where μ_0 is the water permanent dipole moment, $\mathbf{E}'_k = |E'_k|\mathbf{e}'_k$ is the sum of E_k and the average dipoles of all other water dipoles. An equation of the form of eq 9 was first obtained by Langevin in treating classically the magnetic susceptibility of an ensemble of noninteracting, orientable permanent magnetic dipoles using Boltzmann statistics.[22] The analogous equation for electric dipoles was subsequently obtained by Debye in treating the dielectric constant of an ensemble of noninteracting orientable permanent electric dipoles.[22] Equation 9 is an extension of the Langevin−Debye equation to the case of interacting, orientable permanent electric dipoles.[23]

The interaction of the cluster and the continuum water, v_B, is given by

$$v_B = -\frac{1}{2}\frac{Q^2}{r_L}\left(1 - \frac{1}{\epsilon_w}\right) - \frac{1}{2}\frac{\mu^2}{{r_L}^3}\left(\frac{2\epsilon_w - 2}{2\epsilon_w + 1}\right) \tag{11}$$

where Q and μ are the protein charge and dipole moment respectively and ϵ_w is the bulk dielectric constant of water.

3. Implementation and Parameters

The implementation of the PDLD method used in the studies reported here is incorporated in the program POLARIS, most recently described and documented by Lee, Chu, and Warshel.[18]

The calculation starts from a protein structure, usually in Brookhaven PDB file format. This structure is first converted to a form suitable for PDLD calculations. This involves (i) the deletion of unwanted atoms and (ii) the addition of missing atoms. All crystallographic water molecules are deleted. In addition, exogenous ions and molecules (e.g. Cl^-, SO_4^{2-}, etc.) and, where questionable, chemical modifications of amino acid side chains, are removed. Subsequently, H atoms are added, using "standard" bond lengths, bond angles, and torsional angles. All acidic and basic side chains are constructed in their neutral form. If coordinates were not reported for side chain atoms, they are added, again using "standard" geometrical parameters. In the case of side chains capable of "free" rotation, the relative (Coulombic) energies of four orientations are evaluated (see below) and the configuration of minimum energy selected. In the case of histidine residues, the relative energies of the N_δ- and N_ϵ-protonated forms are evaluated similarly and the configuration of minimum energy again selected.

Table 1. [Fe-S] Cluster Charges[a]

cluster	atom	charge: oxidized	charge: reduced
$FeCys_4^{1-/2-}$	Fe	−0.05	−0.38
	Sγ	−0.2375	−0.405
$Fe_2S_2Cys_4^{2-/3-}$ [b]	Fe	−0.02	−0.07
			−0.15
	Sγ	−0.28	−0.365
			−0.455
	S*	−0.42	−0.57
$Fe_3S_4Cys_3^{2-/3-}$	Fe	−0.057	−0.109
	Sγ	−0.203	−0.339
	S*	−0.305	−0.414
$Fe_4S_4Cys_4^{1-/2-}$	Fe	−0.005	−0.05
	Sγ	−0.065	−0.18
	S*	−0.18	−0.27
$Fe_4S_4Cys_4^{2-/3-}$	Fe	−0.05	−0.095
	Sγ	−0.18	−0.295
	S*	−0.27	−0.36

[a] Derived from X_α density functional calculations.[24] [b] Upper and lower charges in the 3− cluster are for the "Fe^{3+}" and "Fe^{2+}" sites, respectively (see text).

Next, charges are assigned to all protein atoms. The charges of the [Fe-S] cluster sum to the net charge and depend on the cluster oxidation level. The values used in the studies described below are given in Table 1. They are obtained from *ab initio* density functional theory (DFT) calculations.[24] (Note that the results of PDLD calculations are fairly insensitive to the specific atom charges adopted.[9]) All other atoms are assigned "standard" charges, with two exceptions: (i) the β-CH_2 and α-CH moieties of ligating cysteine residues are uncharged, and (ii) the Fe and S* of other [Fe-S] clusters are uncharged. The Coulombic interactions of the $Fe_xS_\gamma^*(S_\gamma)_z$ cluster in its oxidized and reduced states with all other protein atoms, $v_{Q\mu}$, are then calculated. (As indicated above, where multiple options are considered for H atom positions, $v_{Q\mu}$ is calculated and the position of lowest energy selected.)

The dipoles induced in the protein atoms (excluding cluster atoms) by the protein charges are then calculated, giving values for $v_{Q\alpha}$ in the oxidized and reduced protein states. Next, the Langevin dipole grid is constructed and v_L calculated. The grid fills a sphere of radius $r_L = 25$ Å and comprises inner and

outer sections: the former has a 1 Å spacing and fills an inner-sphere of radius 12 Å; the latter has a 3 Å spacing and fills the shell between the 12 and 25 Å spheres.[25] Grid points are assigned dipoles as described above. v_L is then calculated, using the previously assigned protein charges and induced dipoles, with the cluster in its oxidized level. The origin of the grid is then varied and v_L recalculated. This is repeated up to a total of 30 grids. The grid providing the largest v_L is selected as the optimum. This grid is then used to calculate v_L for the reduced cluster. Lastly, the bulk dielectric contributions, v_B, are calculated. Note that the calculations of $v_{Q\alpha}$ and v_L are iterative; we use 10 and 30 iterations respectively to achieve adequate convergence.

Changes in Δv (in cal) are related to changes in redox potential, ϵ (in mV), via

$$1000 \text{ cal} = 43.4 \text{ mV} \qquad 1 \text{ mV} = 23.06 \text{ cal}$$

B. PDLD Calculations

PDLD calculations require protein structures i.e. atomic coordinates. Since the earliest structure determinations of proteins containing [Fe-S] clusters—for the prototypical rubredoxin of *Clostridium pasteurianum*,[26] HiPIP of *Chromatium vinosum*,[27] and low-potential ferredoxin of *Peptococcus aerogenes*[27]—the number of such structures has increased steadily. Until recently, structures were exclusively derived via X-ray crystallography; very recently, NMR structures have begun to be reported. Table 2 lists the proteins containing [Fe-S] clusters whose structures have been determined to date and details the Brookhaven Protein Data Base (PDB) file names of the structures (where available), for X-ray structures the resolution of the diffraction data, and specific relevant features of the structures. In some cases, initially reported X-ray structures have been improved by the use of new data at higher resolution and/or by further refinement. In such cases, Table 2 lists only the most recent (and, presumably, accurate) structure. In three cases—*Pf*Rd, *Cv*HiPIP, and *Av*FdI—X-ray structures have been reported for both oxidized and reduced proteins. In two cases—*Ca*Fd and *Av*FdI—X-ray structures have been reported by two different groups. In a number of cases, crystal unit cells contain more than one independent protein molecule and multiple structures result.

Table 2 also lists the redox potentials, where known, of the proteins whose structures have been determined. Redox potentials depend on many parameters, including pH, temperature, buffer, ionic strength, and method of measurement. For many proteins, redox potentials have only been measured by a single method and for a single set of experimental parameters. In a few cases, the variation of redox potential with experimental variables has been more extensively studied. In general, over the ranges studied variations are tens of millivolts in order of magnitude. This should be borne in mind when comparing redox potentials of different proteins measured by different methods and/or under different experimental conditions.

Comparison of PDLD calculations of redox potentials of [Fe-S] proteins containing a specific type of cluster to experiment requires that there exist two or more proteins whose structures and redox potentials are known. At this time, this requirement is met in the case of the $FeCys_4$, $Fe_2S_2Cys_4$, $Fe_3S_4Cys_3$, and $Fe_4S_4Cys_4$ clusters. To date, there are insufficient structures of proteins containing clusters heterogeneous with respect to either metal content or ligation.

Fe Cys_4 Proteins. Proteins containing the Fe Cys_4 cluster are referred to as rubredoxins. The name originates in their characteristic red color when the cluster is in its oxidized, 1−, state. Structures have been reported for seven proteins containing $FeCys_4$ clusters. Here, we consider the five rubredoxins: *Cp*Rd, *Dd*Rd, *Dg*Rd, *Dv*Rd, and *Pf*Rd. They are all bacterial and very similar in size (45−54 amino acids). All contain two Cys-X_2-Cys sequences which together provide the four ligands of the cluster. The second Cys of each binding region is followed by Gly. Due to their relatively small size, X-ray structures have in all cases been obtained at relatively high resolution (1.0−1.8 Å). In one case, *Pf*Rd, X-ray structures were determined in both oxidized and reduced states; all other structures are for oxidized proteins.

The 1−/2− redox potentials of these five rubredoxins listed in Table 2 lie within an extremely narrow range: −60 to +5 mV. Note that the value for *Pf*Rd is for 25 °C; above ∼50 °C, the potential of *Pf*Rd drops rapidly with increasing temperature, being <−150 mV at 90 °C.[78]

The results of PDLD calculations on *Cp*Rd, *Dd*Rd, *Dg*Rd, *Dv*Rd, and *Pf*Rd are given in Table 3 and Figure 2. The *N*-formyl groups in *Dd*Rd and *Dg*Rd are removed. In the cases of *Dd*Rd and *Dv*Rd calculations were carried out for the 16 and 8 structures comprising all permutations of disordered residues and the results averaged. In the case of *Pf*Rd, calculations were carried out using the oxidized structure (1CAA).

$Fe_2S_2Cys_4$ Proteins. Structures have been reported for nine proteins containing $Fe_2S_2Cys_4$ clusters. Here we consider the four proteins: *An*hetFd, *An*vegFd, *Ea*FdI, and *Sp*Fd. They are all plant or algal proteins and very similar in size (95−98 amino acids). All contain one Cys-X_4-Cys-X_2-Cys sequence which provides three of the four Cys cluster ligands; the fourth Cys ligand is distant in the sequence. The resolution of the X-ray structures varies from 1.7 to 2.5 Å. All structures were determined in the oxidized state.

The 2−/3− redox couple potentials of the four ferredoxins lie within a very narrow range: −380 to −440 mV. Note that the potential of *Ea*FdI is questionable (Table 2, footnote *j*).

The results of PDLD calculations on *An*hetFd, *An*vegFd, *Ea*FdI, and *Sp*Fd are given in Table 4 and Figure 3. In the cases of *An*vegFd, and *Ea*FdI there are two independent molecules in the unit cell and, hence, two structures. In each case, calculations were carried out for both structures and the results averaged.

The reduced 3−, state of the $Fe_2S_2Cys_4$ cluster is "valence-localized (trapped)" i.e. one Fe is 2+, the other is 3+. NMR studies have shown that in *Sp*Fd

Table 2. Structures and Redox Potentials of Proteins Containing [Fe-S] Clusters

[Fe-S] cluster	protein	other cofactors	resolution (Å)	ref	Brookhaven (PDB) filename	observed couple	observed potential (mV vs SHE)	ref
$FeCys_4$	*Clostridium pasteurianum* rubredoxin (*Cp*Rd)		1.2	28	4RXN; 5RXN[a]	1−/2−	−60	74
	Desulfovibrio desulfuricans strain 27774 rubredoxin (*Dd*Rd)		1.5	29	6RXN[b]		∼0	75
	Desulfovibrio gigas rubredoxin (*Dg*Rd)		1.4	30	1RDG[c]		5	76
	Desulfovibrio vulgaris strain Hildenborough rubredoxin (*Dv*Rd)		1.0	31	8RXN[d]		5[e]	77
	Pyrococcus furiosus rubredoxin (*Pf*Rd)		1.8	32	1CAA; 1CAD[f]		0	78
	Desulfovibrio vulgaris rubrerythrin	Fe−O−Fe center	2.1	33			200	79
	Desulfovibrio gigas desulforedoxin		1.8	34			−35	80
$Fe_2S_2Cys_2$	*Anabaena* 7120 heterocyst ferredoxin (*An*hetFd)		1.7	35	1FRD	2−/3−	−405	81
	Anabaena 7120 vegetative ferredoxin (*An*vegFd)		1.7	36	HHA[g]		−440	81
	Aphanothece sacrum ferredoxin I (*As*FdI)		2.2	37	1FXI[h]			
	Equisetum arvense ferredoxin I (*Ea*FdI)		1.8	38	1FRR[i]		−405[j]	82
	Spirulina platensis ferredoxin (*Sp*Fd)		2.5	39	4FXC		−380	82
	Halobacterium marismortui ferredoxin		2.5	40				
	Pseudomonas putida ferredoxin (putidaredoxin)		*k*	41	1PUT[l]		−230	83
	Pseudomonas cepacia phthalate dioxygenase reductase	FMN	2.0	42	1PIA		−175	42
	Desulfovibrio gigas aldehyde oxido-reductase[m]	Mo-pterin	2.25	43			−260, −285[n]	84
$Fe_3S_4Cys_3$	*Azotobacter vinelandii* ferredoxin I (*Av*FdI)	$Fe_4S_4Cys_4$	2.3	44	1FER[o]	2−/3−		
			1.9	45	4FDI[p]		−425	85
			1.9−2.2	46	5FDI; 1FDC; 1FDA; 1FDB[q]			
	Desulfovibrio gigas ferredoxin II (*Dg*FdII)		1.7	47	1FXD[r]		−130	86
	pig heart aconitase		2.1	48	5ACN[s]		−160[t]	87
	Desulfovibrio gigas hydrogenase	NiFe cluster, $Fe_4S_4Cys_4$, $Fe_4S_4Cys_3His$	2.85	49			−70	88
$Fe_4S_4Cys_4$	*Chromatium vinosum* HiPIP (*Cv*HiPIP)		2.0	50	1HIP[u]	1−/2−	360	89
	Ectothiorhodospira halophila HiPIP isoform I (*Eh*HiPIP)		1.7	51	HHH[i]		120	90
	Ectothiorhodospira vacuolata HiPIP isoform II (*Ev*HiPIP)		1.8	52	1HPI		170	91
	Rhodocyclus tenuis HiPIP strain 2761 (*Rt*HiPIP)		1.5	53	1ISU[i]		300	92
	Chromatium vinosum HiPIP		*k*	54	1HRQ, 1HRR[v]		360	89
	Ectothiorhodospira halophila isoform I HiPIP		*k*	55	1PIH, 1PIJ[w]		120	90
$Fe_4S_4Cys_4$	*Azotobacter vinelandii* ferredoxin I (*Av*FdI)	$Fe_3S_4Cys_3$	2.3	44	1FER[o]	2−/3−		
			1.9	45	4FDI[p]		−650	85
			1.9−2.2	46	5FDI; 1FDC; 1FDA; 1FDB[q]			
	Bacillus thermoproteolyticus ferredoxin (*Bt*Fd)		2.3	56	2FXB		−280[x]	93
	Clostridium acidi-urici ferredoxin (*Ca*Fd)[y]		1.8	57	1FDN;[z]		−420	94
			1.8	58	1FCA[z]			
	Desulfovibrio africanus ferredoxin I (*Da*FdI)		2.3	59	1FXR[i]		−385	95
	Peptococcus aerogenes ferredoxin (*Pa*Fd)[y]		2.0	60	ETA1[aa]		−430	94
	Azotobacter vinelandii nitrogenase Fe protein (*Av*2)		2.9	61	1NIP[ab]		−280	96
	Clostridium pasteurianum nitrogenase Fe protein (*Cp*2)			62			−265	96
	Pyrococcus furiosus aldehyde oxidoreductase	W-pterin	2.3	63	1AOR[ac]		∼−600[ad]	78

Table 2. (Continued)

[Fe-S] cluster	protein	other cofactors	resolution (Å)	ref	Brookhaven (PDB) filename	observed couple	observed potential (mV vs SHE)	ref
	bacterium W3A1 trimethylamine dehydrogenase	FMN	2.4	64	2TMD[ae]		0	97
	Bacillus subtilis glutamine 5-phosphoribosyl-1-pyrophosphate aminotransferase		3	65	1GPH[af]		<−600	98
	Desulfovibrio gigas hydrogenase	Ni-Fe cluster, $Fe_3S_4Cys_3$, $Fe_4S_4Cys_3His$	2.85	49			−290, −330[ag]	99
	Clostridium pasteurianum ferredoxin[y]		*k*	66			−390	100
	Azotobacter vinelandii ferredoxin I mutants	$Fe_3S_4Cys_3$						
	F2Y		2.1	67	1FRH		−650	67
	D15N		1.9	68	1FDD		−650	68
	C20S		2.5	69	1FRX		−690	69
	C20A		1.9	70	1FD2		−750	85
	D23N		2.1	67	1FRI		−650	67
	C24A		2.0	71	2FD2		−600	85
	F25I		2.3	67	1FRJ[ah]		−670	67
	H35D		1.9	67	1FRK		−650	67
	E38S		2.0	67	1FRL		−650	67
	E46A		2.0	67	1FRM		−650	67
	Escherichia coli endonuclease III (*Ec*EnIII)		2.0	72	2ABK[ai]			
$Fe_4S_4Cys_3$	pig heart aconitase		2.5	73	6ACN; 1AMI; 1AMJ; 1NIT; 7ACN; 8ACN[aj]		−500	87

[a] Hydrogens are included for each amino acid. 4RXN and 5RXN result from unconstrained and constrained refinements respectively. [b] There are two sets of coordinates for residues E12, Q25, C31, and K39, each with 50% occupancy. The N-terminal Met is N-formylated. [c] The N terminal Met is N-formylated. [d] There are two sets of coordinates for residues E12, D21, and P15; occupancies are 50%, 50%, and 75%:25% respectively. One SO_4^{2-} is also present. [e] This potential is for *Dv* strain Miyazaki Rd which is the S29A, D31E, L33V, V41I mutant of *Dv* strain Hildenborough Rd. [f] 1CAA and 1CAD are structures of oxidized and reduced *Pf*Rd, respectively. [g] There are two molecules in the crystal unit cell; one has 2-methyl-2,4-pentanediol bound to its exterior. [h] There are four molecules in the crystal unit cell. [i] There are two molecules in the crystal unit cell. [j] This redox potential is for a ferredoxin from *Equisetum telmateia*. Two ferredoxins (I and II) have been purified from both *E. telmateia* and *E. arvense*. There is only one difference between the sequences of the analogous ferredoxins from *E. telmateia* and *E. arvense*;[101] unfortunately, it is not stated in ref 82 which *Et* ferredoxin is studied. [k] NMR structure; resolution not applicable. [l] The file contains 12 NMR structures. [m] There are two $Fe_2S_2Cys_4$ clusters. [n] In ref 102, three redox couples were reported for EPR signals IA, IB, and II. In ref 84, EPR signals IA and IB were shown to derive from the same cluster. It is not yet known which cluster has the lower redox potential. [o] Oxidized *Av*FdI at pH 6.5. There are two sets of coordinates for D58 and E66; each have 60%:40% occupancy. [p] Oxidized *Av*FdI at pH 8.0. [q] 5FDI, 1FDC, 1FDA, and 1FDB are oxidized pH 8, reduced pH 8, oxidized pH 6, and reduced pH 6 structures, respectively. In reduced *Av*FdI, the $Fe_3S_4Cys_4$ and $Fe_4S_4Cys_4$ clusters are reduced (3−) and oxidized (2−) respectively. [r] Cys11 is thiomethylated in this structure. [s] The structure contains a SO_4^{2-} bound to the active site, and a tricarballylate inhibitor ion bound to the entrance of the solvent cleft that extends to the active site. [t] This redox potential is for bovine heart aconitase. [u] This structure is for oxidized *Cv*HiPIP. The coordinates for residues K18, S26, A32, and Q50 are incomplete. [v] NMR structures. The file 1HRQ contains a single "best fit" structure while 1HRR contains 15 structures. [w] NMR structures. The file 1PIH contains a single "best fit" structure while 1PIJ contains 15 structures. [x] This redox potential is for *Bacillus stearothermophilus* ferredoxin (*Bs*Fd). *Bs*Fd is the D64E; E81D mutant of *Bt*Fd.[103] [y] There are two $Fe_4S_4Cys_4$ clusters; their redox potentials are indistinguishable. [z] The cluster ligated by Cys 8, 11, 14, and 47 is defined as cluster I; the cluster ligated by Cys 18, 37, 40, and 43 is defined as cluster II. 1FDN has two sets of coordinates given for N21; each with 50% occupancy; 1FCA has four sequence differences with respect to 1FDN: 1FCA substitutes N21, S25, D27, and D28 of 1FDN by D21, Q25, G27, and S28. [aa] The cluster ligated by Cys 8, 11, 14, and 46 is defined as cluster I; the cluster ligated by Cys 18, 36, 39, and 42 is defined as cluster II. [ab] There is one homodimer present in the crystal unit cell. Molybdate is present in the putative ATP binding site. One ADP per homodimer is present with an occupancy of 50%. [ac] There are two molecules in the unit cell; each has an associated hydrated Na^+ ion. [ad] Two redox couples are reported at −590 and −650 mV. However, there is only one $Fe_4S_4Cys_4$ cluster. [ae] There are two molecules in the unit cell; one ADP is associated with each. [af] There are four molecules in the unit cell; two AMP are associated with each. [ag] It has not been determined which potential belongs to the $Fe_4S_4Cys_4$ cluster. [ah] There are two sets of coordinates for the side chain of I32, each with 50% occupancy. [ai] Reversible redox behavior has not been definitively observed.[104] [aj] 8ACN contains a SO_4^{2-} bound to the active site. A tricarballylate inhibitor molecule is bound to the solvent cleft that extends to the active site. 1AMI represents the structure of pig heart aconitase complexed with α-methyl-isocitrate; 1AMJ is complexed with sulfate and hydroxide; 1NIS is complexed with nitrocitrate; 1NIT is complexed with sulfate; 7ACN is complexed with isocitrate; 8ACN is complexed with nitroisocitrate.

Table 3. $FeCys_4$ Proteins (Rubredoxins)[a]

	*Cp*Rd[b]		*Dd*Rd		*Dg*Rd		*Dv*Rd		*Pf*Rd	
	PDLD	MD-PDLD	PDLD	MD-PDLD	PDLD	MD-PDLD	PDLD	MD-PDLD	PDLD	MD-PDLD
$\Delta\upsilon_{Q\mu}$	70.36	71.62	70.18	75.84	70.42	72.26	72.33	71.69	74.54	74.56
$\Delta\upsilon_{Q\alpha}$	19.41	19.41	19.8	17.56	18.45	18.89	18.86	18.62	18.85	17.73
$\Delta\upsilon_{L}$	54.17	57.61	58.11	55.93	58.92	57.56	62.43	61.78	60.65	56.98
$\Delta\upsilon_{B}$	18.4	19.53	19.02	19.43	19.78	19.6	20.2	19.84	19.86	19.02
$\Delta\upsilon$	162.34	168.17	167.11	168.76	167.57	168.31	173.82	171.93	173.9	168.29
$\Delta\Delta\upsilon$	0	0	4.77	0.59	5.23	0.14	11.48	3.76	11.56	0.12
ϵ_{calc}[c]	−60	−60	147	−34	167	−54	438	103	441	−55
$\Delta\upsilon_{QQ}$		−2.22		−0.82		−0.86		−1.3		−1.38
$\Delta\Delta\upsilon_{QQ}$		0		1.4		1.36		0.92		0.84
$\Delta\epsilon_{calc}$		0		61		59		40		36
ϵ_{obs}	−60		0		5		5		0	

[a] $\Delta\upsilon$ in kcal; ϵ in mV. [b] 5RXN. [c] *Cp*Rd is chosen as the reference protein.

Table 4. $Fe_2S_2Cys_4$ Proteins[a]

	*An*HetFd		*An*VegFd		*Ea*FdI		*Sp*Fd		*As*FdI	
	PDLD	MD-PDLD	PDLD	MD-PDLD	PDLD	MD-PDLD	PDLD	MD-PDLD	PDLD	MD-PDLD
$\Delta\upsilon_{Q\mu}$	114.07	119.63	119.35	119.97	122.2	118.09	91.7	115.55	104.04	119.49
$\Delta\upsilon_{Q\alpha}$	31.31	28.73	28.69	26.52	25.49	24.43	40.55	29.85	38.31	28.1
$\Delta\upsilon_{L}$	58.42	58.29	58.4	55.94	59.29	62.95	63.79	60.76	59.29	59.07
$\Delta\upsilon_{B}$	31.08	32.35	31.63	30.85	32.9	32.34	32.15	32.13	31.76	32.34
$\Delta\upsilon$	234.88	239	238.07	233.28	239.88	237.81	228.19	238.29	233.4	239
$\Delta\Delta\upsilon$	0	0	3.19	−5.72	5	−1.19	−6.69	−0.71	−1.48	0
ϵ_{calc}[b]	−405	−405	−267	−653	−188	−457	−695	−436	−469	−405
$\Delta\upsilon_{QQ}$		−2.22		−3.52		−2.63		−3.87		−3.77
$\Delta\Delta\upsilon_{QQ}$		0		−1.3		−0.41		−1.65		−1.55
$\Delta\epsilon_{calc}$		0		−50		−16		−63		−60
ϵ_{obs}	−405		−440		−405		−380			

[a] $\Delta\upsilon$ in kcal; ϵ in mV. [b] *An*HetFd is chosen as the reference protein.

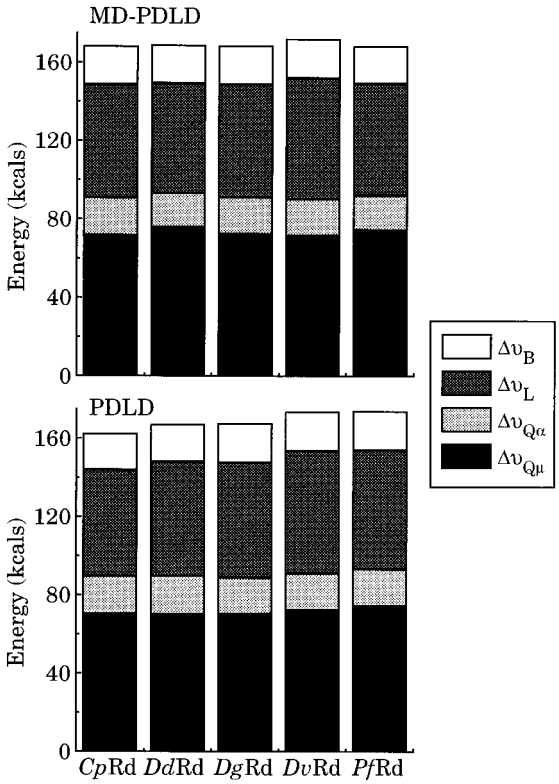

Figure 2. PDLD calculations for $FeCys_4$ clusters. Components of $\Delta\upsilon$ are calculated with (MD-PDLD) and without (PDLD) molecular dynamics averaging.

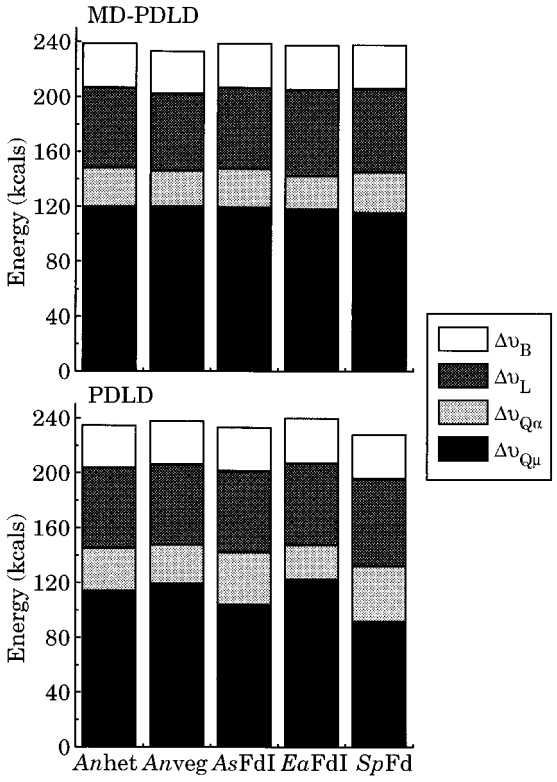

Figure 3. PDLD calculations for $Fe_2S_2Cys_4$ clusters. Components of $\Delta\upsilon$ are calculated with (MD-PDLD) and without (PDLD) molecular dynamics averaging.

and *Porphyra umbilicalis* ferredoxin it is the Fe ligated by the two Cys separated by four residues in the Cys-X_4-Cys-X_2-Cys motif which is reduced.[105] Our calculations are based on the assumption that this is the case in all four proteins.

$Fe_3S_4Cys_3$ Proteins. Structures have been reported for four proteins containing $Fe_3S_4Cys_3$ clus-

Table 5. $Fe_3S_4Cys_4$ Proteins[a]

	*Av*FdI		*Dg*FdII	
	PDLD	MD-PDLD	PDLD	MD-PDLD
$\Delta v_{Q\mu}$	96.79	95.77	84.26	84.3
$\Delta v_{Q\alpha}$	31.23	31.72	32.93	29.49
Δv_L	36.76	36.66	62.5	57.52
Δv_B	30.54	31.16	31.31	31.36
Δv	195.32	195.31	211	202.67
$\Delta\Delta v$	0	0	15.68	7.36
ϵ_{calc}	−425	−425	255	−106
Δv_{QQ}		−4.25		−4.37
$\Delta\Delta v_{QQ}$		0		−0.12
$\Delta\epsilon_{calc}$[b]		0		−5
ϵ_{obs}	−425		−130	

[a] Δv in kcal; ϵ in mV. [b] *Av*FdI is chosen as the reference protein.

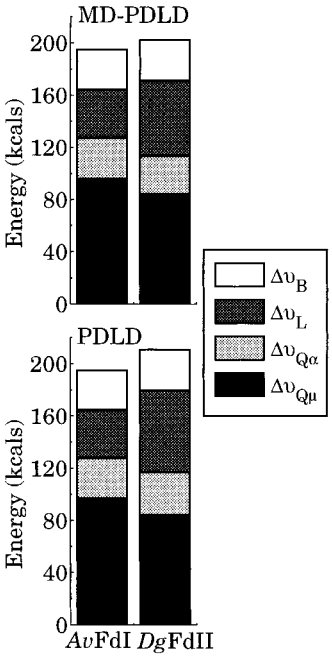

Figure 4. PDLD calculations for $Fe_3S_4Cys_3$ clusters. Components of Δv are calculated with (MD-PDLD) and without (PDLD) molecular dynamics averaging.

ters. Here we consider the two proteins: *Av*FdI and *Dg*FdII. In *Dg*FdII, the $Fe_3S_4Cys_3$ cluster is the only prosthetic group; in *Av*FdI, a $Fe_4S_4Cys_4$ cluster is also present. The two proteins differ significantly in size and do not possess a common sequence motif containing either two or three Cys ligands. The resolution of the X-ray structure of *Dg*FdII is 1.7 Å. The structure of *Dg*FdII is for the oxidized state. X-ray structures of *Av*FdI have been reported by two groups. Merritt et al. reported a 2.3 Å structure at pH 6.5.[44] Stout[45,46] reported structures with the $Fe_3S_4Cys_3$ cluster in both oxidized and reduced states and at two pH values: 6 and 8; in all structures the $Fe_4S_4Cys_4$ cluster is in the same, 2−, oxidation level.

The potentials of the 2−/3− redox couple of *Av*FdI and *Dg*FdII, −420 and −130 mV respectively, differ significantly. The potential of the $Fe_3S_4Cys_3$ cluster of *Av*FdI exhibits substantial pH dependence.[85] Spectroscopic studies[106] have shown that this originates in protonation of the reduced protein at low pH; the p*K* is in the range 7−8.[85,106]

The results of PDLD calculations on *Av*FdI and *Dg*FdII are given in Table 5 and Figure 4. In the case of *Dg*FdII, C11 was reported to be chemically modified (thiomethylated). Subsequent NMR studies are consistent with an unmodified C11.[107] We have therefore deleted the extra thiomethyl atoms from the PDB file. Calculations on *Av*FdI used the oxidized, pH 8 structure 4FD1.

$Fe_4S_4Cys_4$ Proteins. The $Fe_4S_4Cys_4$ cluster may express either the 1−/2− redox couple or the 2−/3− redox couple. To date, all potentials of the 1−/2− couple are > 0 mV, while all potentials of the 2−/3− couple are < 0 mV.[108] Accordingly, proteins expressing the 1−/2− couple have been named HiPIPs (high-potential iron proteins). Those expressing the 2−/3− couple are sometimes referred to as low-potential ferredoxins.

Structures have been reported for four HiPIPs: *Cv*, *Eh*, *Ev*, and *Rt*. They are all bacterial and fairly similar in size (62−85 amino acids). All contain a single Cys-X_2-Cys sequence providing two of the four cluster ligands; the other two Cys ligands are distant. The resolutions of their X-ray structures lie in the range 1.5−2.0 Å. In the case of *Cv*HiPIP, X-ray structures were obtained for both oxidized and reduced states;[27] for the other HiPIPs, oxidation states were not defined.[109]

The potentials of the 1−/2− redox couple of the four HiPIPs span the range +120 to +360 mV. In the case of the *Cv*-, *Ev*-, and *Rt*HiPIPs, thorough studies of the pH, ionic strength and temperature dependences of the potentials were recently reported.[91]

The results of PDLD calculations for the 1−/2− $Fe_4S_4Cys_4$ cluster redox couple on *Cv*-, *Eh*-, *Ev*-, and *Rt*HiPIPs are given in Table 6 and Figure 5. In both *Eh*- and *Rt*HiPIPs there are two independent molecules in the unit cell and, hence, two structures. In both cases, calculations were carried out for each structure and the results averaged. The calculations for *Cv*HiPIP use the oxidized structure (1HIP). Four residues were incompletely defined in this structure: K18, S26, A32 and Q50. Coordinates for the side chains of these residues were obtained via molecular modeling.

Structures have been reported for 12 proteins containing $Fe_4S_4Cys_4$ clusters expressing the 2−/3− couple. Here we consider the five proteins: *Av*FdI, *Bt*Fd, *Ca*Fd, *Da*FdI, and *Pa*Fd. All are bacterial. They vary significantly in size (55−106 amino acids). Two contain a single $Fe_4S_4Cys_4$ cluster and no other prosthetic group: *Bt*Fd and *Da*FdI. Two contain two $Fe_4S_4Cys_4$ clusters: *Pa*Fd and *Ca*Fd. One contains one $Fe_4S_4Cys_4$ and one $Fe_3S_4Cys_3$ cluster: *Av*FdI. A Cys-X_2-Cys-X_2-Cys sequence provides three of the four Cys ligands of each $Fe_4S_4Cys_4$ cluster, the fourth Cys ligand being distant. The resolutions of their X-ray structures lie in the range 1.8−2.3 Å. X-ray structures of *Pa*Fd, *Bt*Fd, *Ca*Fd, and *Da*FdI were determined in their oxidized states. As discussed above, the structure of *Av*FdI has been determined in two oxidation states and at two pH values. In all cases the $Fe_4S_4Cys_4$ cluster is in the oxidized, 2− state.

The potentials of the 2−/3− redox couples of the five proteins span the range −650 to −280 mV. In the cases of *Pa*Fd and *Ca*Fd, the experimental redox potentials of the two clusters are indistinguishable.

Table 6. HiPIP Proteins[a]

	*Cv*HiPIP		*Eh*HiPIP		*Ev*HiPIP		*Rt*HiPIP	
	PDLD	MD-PDLD	PDLD	MD-PDLD	PDLD	MD-PDLD	PDLD	MD-PDLD
$\Delta v_{Q\mu}$	35.84	26.88	39.6	28.75	23.75	19.29	37.38	27.99
$\Delta v_{Q\alpha}$	24.84	27.77	23.82	28.24	32.43	33.38	21.19	23.01
Δv_{L}	34.02	31.52	24.55	23.08	36.13	31.81	38.54	37.87
Δv_{B}	19.72	19.25	19.74	19.26	19.94	18.97	19.45	19.02
Δv	114.42	105.42	107.71	99.33	112.25	103.45	116.56	107.89
$\Delta\Delta v$	0	0	−6.71	−6.09	−2.17	−1.97	2.14	2.47
ϵ_{calc}[b]	360	360	69	96	266	275	453	467
Δv_{QQ}		0.17		−1.35		−0.72		1.45
$\Delta\Delta v_{QQ}$		0		−1.52		−0.89		1.28
$\Delta\epsilon$		0		−66		−39		56
ϵ_{obs}	360		120		170		300	

[a] Δv in kcal; ϵ in mV. [b] *Cv*HiPIP is chosen as the reference protein.

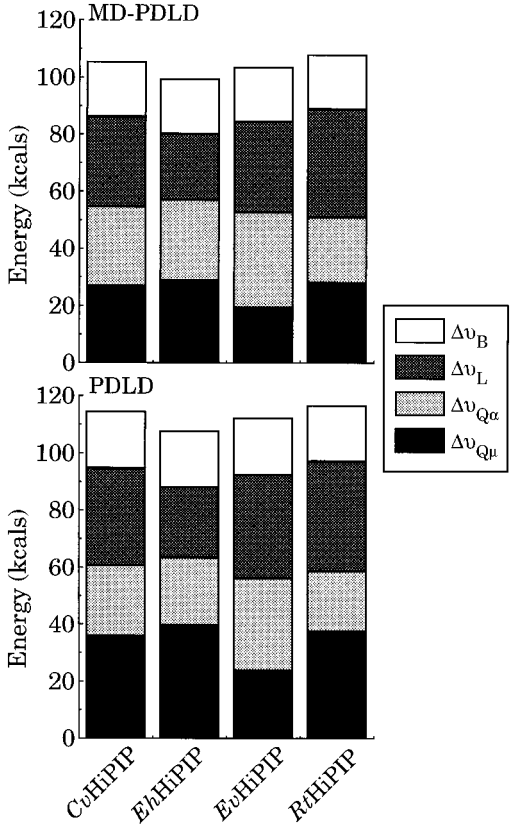

Figure 5. PDLD calculations for $Fe_4S_4Cys_4^{1-/2-}$ clusters. Components of Δv are calculated with (MD-PDLD) and without (PDLD) molecular dynamics averaging.

The results of PDLD calculations for the 2−/3− $Fe_4S_4Cys_4$ cluster redox couple on *Av*FdI, *Bt*Fd, *Ca*Fd, *Da*FdI, and *Pa*Fd are given in Table 7 and Figure 6. In the case of *Da*FdI there are two independent molecules in the unit cell. Calculations were carried out for the two structures and the results averaged. In the case of *Ca*Fd, the structure of Duee et al. (IFDN) was used; calculations were carried out for both orientations of N21 and the results averaged. In the case of *Av*FdI, the oxidized, pH 8 structure 4FD1 of Stout was used.

In addition to PDLD calculations on expressed redox couples of proteins containing $Fe_4S_4Cys_4$ clusters, we have also carried out a limited number of calculations on unexpressed redox couples. Specifically: we have carried out calculations for the 1−/2− couple of the low-potential ferredoxins *Av*FdI and *Bt*Fd and for the 2−/3− couple of the *Cv*- and *Ev*HiPIPs. The results are given in Tables 8 and 9 and Figure 7.

We now examine the results obtained from the PDLD calculations in more detail. To begin with we discuss the four contributions to Δv individually. Subsequently, we discuss the variations in Δv and the variations in redox potential predicted thence.

We focus first on the $\Delta v_{Q\mu}$ terms. These vary widely. Overall, the range is ∼100 kcal. The lowest values are given by the *Cv*-, *Eh*-, *Ev*-, and *Rt*HiPIPs (20−40 kcal). The highest values are given by the *An*het, *An*veg, *Ea*- and *Sp*ferredoxins (90−130 kcal). $\Delta v_{Q\mu}$ can be partitioned into the contributions of individual amino acid residues as illustrated in Figure 8 for *Cp*Rd, *An*hetFd, *Av*FdI ($Fe_3S_4Cys_3$ cluster), *Cv*HiPIP and *Av*FdI ($Fe_4S_4Cys_4$ cluster). Individual contributions of residues lie in the range 0−12 kcal and can be both positive and negative; for all five proteins, positive contributions predominate. The largest individual contributions originate in residues close to the cluster.

The contributions of individual amino acid residues can be further separated into the contributions of their $C_\alpha H$ + side chain and their amide (NH and CO) components. The contributions of amide groups are also illustrated in Figure 8. It is immediately apparent that they vastly preponderate over the contributions of the $C_\alpha H$ and side-chain groups. A very large fraction of the total $\Delta v_{Q\mu}$ is thus attributable to the amide groups of the protein.

It is not surprising that amide groups yield large $\Delta v_{Q\mu}$ contributions. An amide group has a very large dipole, due to the high polarity of both N−H and C=O bonds and their essentially parallel alignment when the amide group is trans. When (i) close to a charged cluster and (ii) optimally oriented, it is to be expected that the cluster charge−amide dipole interaction is substantial.

The variations in $\Delta v_{Q\mu}$ among proteins can thus, to a good first approximation, be correlated with the structure of the main chain of the polypeptide in the vicinity of the cluster. Proteins, containing a given cluster, which exhibit high structural homology around a cluster can be expected to give very similar $\Delta v_{Q\mu}$ values. Conversely, low homology should lead to substantial differences in $\Delta v_{Q\mu}$. This expectation is borne out. The five rubredoxins studied have very similar main chain structures in the vicinity of the $FeCys_4$ cluster.[28−32] Accordingly, the $\Delta v_{Q\mu}$ values fall in a narrow range: 70−75 kcal. The four $Fe_2S_2Cys_4$

Table 7. Low-Potential $Fe_4S_4Cys_4$ Proteins[a]

	*Av*FdI		*Bt*Fd		*Ca*Fd(I)		*Ca*Fd(II)	
	PDLD	MD-PDLD	PDLD	MD-PDLD	PDLD	MD-PDLD	PDLD	MD-PDLD
$\Delta v_{Q\mu}$	90.83	85.97	67.5	75.14	84.8	89.24	91.67	85.35
$\Delta v_{Q\alpha}$	26.17	27.48	37.73	32.63	24.08	21.99	21.22	23.94
Δv_L	56.46	53.79	66.19	65.81	63.49	58.75	61.85	61.12
Δv_B	32.98	32.23	31.77	33.01	31.71	31.63	31.66	31.57
Δv	206.44	199.47	203.19	206.59	204.08	201.61	206.4	201.98
$\Delta\Delta v$	0	0	−3.25	7.12	−2.36	2.14	−0.04	2.51
ϵ_{calc}[b]	−650	−650	−791	−341	−752	−557	−652	−541
Δv_{QQ}		−4.74		−4.44		−2.29		−2.55
$\Delta\Delta v_{QQ}$		0		0.3		2.45		2.19
$\Delta\epsilon$		0		13		106		95
ϵ_{obs}	−650		−280		−420		−420	

	*Da*FdI		*Pa*Fd(I)		*Pa*Fd(II)	
	PDLD	MD-PDLD	PDLD	MD-PDLD	PDLD	MD-PDLD
$\Delta v_{Q\mu}$	76.52	85.41	93.32	91.12	86.44	88.69
$\Delta v_{Q\alpha}$	26.78	25.6	20.48	21.35	22.73	22.17
Δv_L	60.21	57.06	60.63	59.15	60.38	56.74
Δv_B	32.66	32.05	30.84	31.17	31.48	31.53
Δv	196.17	200.12	205.27	202.79	201.03	199.13
$\Delta\Delta v$	−10.27	0.65	−1.17	3.32	−5.41	−0.34
ϵ_{calc}[b]	−1,095	−622	−701	−506	−885	−665
Δv_{QQ}		−3.51		−1.87		−2.33
$\Delta\Delta v_{QQ}$		1.23		2.87		2.41
$\Delta\epsilon$		53		124		105
ϵ_{obs}	−385		−430		−430	

[a] Δv in kcal; ϵ in mV. [b] *Av*FdI is chosen as the reference protein.

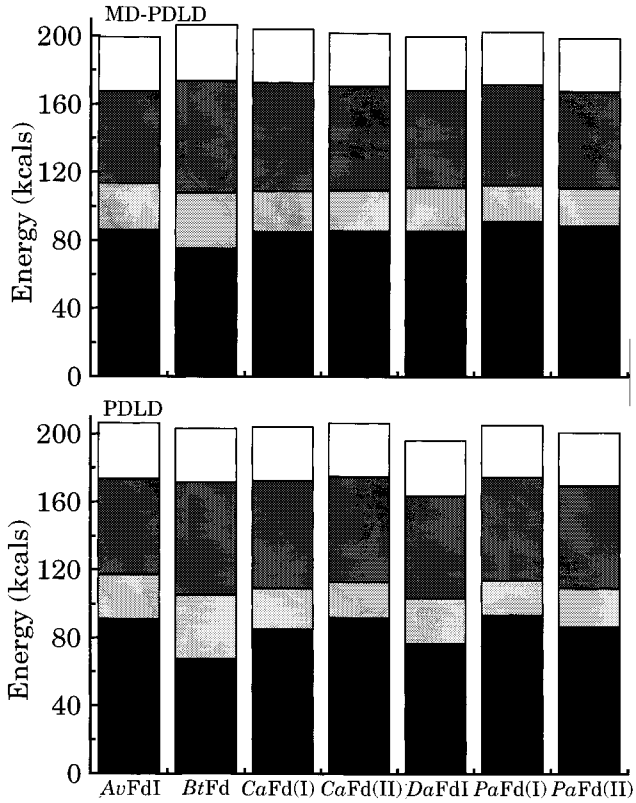

Figure 6. PDLD calculations for $Fe_4S_4Cys_4^{2-/3-}$ clusters. Components of Δv are calculated with (MD-PDLD) and without (PDLD) molecular dynamics averaging. Gray shades are assigned as in Figures 2−5.

ferredoxins exhibit considerable similarity[35,36,38,39] and their $\Delta v_{Q\mu}$ values lie in the range 92−122 kcal. The $Fe_4S_4Cys_4$ proteins exhibit a wide range of $\Delta v_{Q\mu}$ values. For the 1−/2− redox couple, $\Delta v_{Q\mu}$ values for the four HiPIPs lie in the range 24−40 kcal while for *Av*FdI and *Bt*Fd $\Delta v_{Q\mu}$ are 91 and 68 kcal, respectively. For the 2−/3− redox couple, $\Delta v_{Q\mu}$ values for the low-potential ferredoxins, *Av*FdI, *Bt*Fd, *Ca*Fd, *Da*Fd, and *Pa*Fd lie in the range 68−93 kcal while for *Cv*HiPIP and *Ev*HiPIP $\Delta v_{Q\mu}$ are 36 and 24 kcal, respectively. The cluster environments in the HiPIPs are very similar,[50−53] and this is also the case for the five low-potential ferredoxins.[44−46,56−60] In contrast, the cluster environments of the HiPIPs and the low-potential ferredoxins are very different.[27] The much lower values of $\Delta v_{Q\mu}$ for the HiPIPs show the orientations of the amide groups in the environments of the clusters in these proteins are much less favorable than in the low-potential ferredoxins.

We turn now to the $\Delta v_{Q\alpha}$ terms. These are a more complex function of the protein charge distribution than is $\Delta v_{Q\mu}$ and are difficult to partition in a qualitatively useful fashion. Variations of $\Delta v_{Q\alpha}$ among similar proteins tend to be opposite in sign to those in $\Delta v_{Q\mu}$; that is, the sum of $\Delta v_{Q\mu}$ and $\Delta v_{Q\alpha}$ varies less than $\Delta v_{Q\mu}$ alone.

The Δv_L terms originate in water dipoles which fill the space (within the sphere of radius r_L) not occupied by protein atoms. The magnitude of Δv_L depends, first, on the size of the protein: the larger the protein, the smaller the number of water dipoles and, hence, Δv_L. In addition, the magnitude of Δv_L depends on the spatial distribution of the water dipoles. On average, water dipoles close to the cluster will contribute more strongly to Δv_L than those far from the cluster. Thus, the magnitude of Δv_L depends on the closeness of water dipoles to the cluster or, put in another way, the closeness of the cluster to the surface of the protein. For the proteins we have studied, Δv_L values range from 25 to 70 kcal. The lowest values are for the four HiPIPs, whose Δv_L values of 25 to 39 kcal reflect the relatively buried

Table 8. Predictions for the 1−/2− Redox Couple of $Fe_4S_4Cys_4$ Proteins[a]

	*Cv*HiPIP		*Av*FdI		*Bt*Fd		*Ec*EnIII	
	PDLD	MD-PDLD	PDLD	MD-PDLD	PDLD	MD-PDLD	PDLD	MD-PDLD
$\Delta v_{Q\mu}$	35.84	26.88	90.82	76.89	67.5	63.61	15.79	10.65
$\Delta v_{Q\alpha}$	24.84	27.77	−0.09	5.54	12.76	11.97	31.46	32.37
Δv_L	34.02	31.52	32.75	28.77	39.76	40.14	45.42	43.32
Δv_B	19.72	19.25	20.73	19.81	19.43	19.96	19.4	19.2
Δv	114.42	105.42	144.21	131.01	139.45	135.68	112.07	105.54
$\Delta\Delta v$	0	0	29.79	25.59	25.03	30.26	−2.35	0.12
ϵ_{calc}[b]	360	360	1,652	1,470	1,445	1,672	258	365
ϵ_{obs}	360							

[a] Δv in kcal; ϵ in mV. [b] *Cv*HiPIP is chosen as the reference protein.

Table 9. Predictions for the 2−/3− Redox Couple of $Fe_4S_4Cys_4$ Proteins[a]

	*Av*FdI		*Cv*HiPIP		*Ev*HiPIP		*Ec*EnIII	
	PDLD	MD-PDLD	PDLD	MD-PDLD	PDLD	MD-PDLD	PDLD	MD-PDLD
$\Delta v_{Q\mu}$	90.82	85.97	35.84	40.25	23.75	29.68	15.79	17.16
$\Delta v_{Q\alpha}$	26.17	27.48	52.51	49.64	59.99	55.47	58.98	56.18
Δv_L	56.46	53.79	53.84	51.47	55.8	52.62	67.17	64.52
Δv_B	32.98	32.23	32.3	31.8	32.03	31.34	31.86	31.56
Δv	206.43	199.47	174.49	173.16	171.57	169.11	173.8	169.42
$\Delta\Delta v$	0	0	−31.94	−26.31	−34.86	−30.36	−32.63	−30.05
ϵ_{calc}[b]	−650	−650	−2035	−1791	−2162	−1967	−2065	−1953
ϵ_{obs}	−650							

[a] Δv in kcal; ϵ in mV. [b] *Av*FdI is chosen as the reference protein.

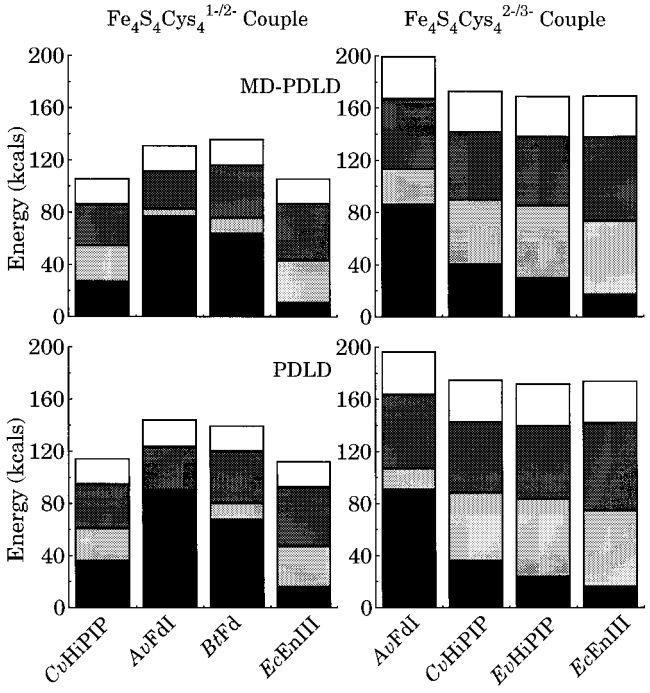

Figure 7. PDLD calculations for $Fe_4S_4Cys_4$ clusters: (left) PDLD and MD-PDLD calculations for the 1−/2− redox couple comparing *Av*FdI, *Bt*Fd, and *Ec*EnIII with *Cv*HiPIP, and (right) PDLD and MD-PDLD calculations for the 2−/3− redox couple comparing *Cv*HiPIP, *Ev*HiPIP, and *Ec*EnIII with *Av*FdI. Gray shades are assigned as in Figures 2−5.

nature of their $Fe_4S_4Cys_4$ clusters. For all other proteins (with the one exception of *Av*FdI ($Fe_3S_4Cys_3$)) Δv_L is > 50 kcal, reflecting the proximity of their clusters to the protein surface. A more detailed picture of the relationship between the distances of water dipoles from the cluster and their contributions to Δv_L is provided by the radial distribution plot in which the contribution to Δv_L of all dipoles within a sphere of radius *r* around the cluster is plotted versus *r*. Radial distributions of Δv_L for *Cp*Rd, *An*hetFd, *Av*FdI ($Fe_3S_4Cys_3$ cluster), *Cv*HiPIP, and *Av*FdI ($Fe_4S_4Cys_4$ cluster) are given in Figure 9. The greater distance of the $Fe_4S_4Cys_4$ cluster of *Cv*HiPIP from the protein surface relative to the $FeCys_4$, $Fe_2S_2Cys_4$, and $Fe_4S_4Cys_4$ clusters of *Cp*Rd, *An*hetFd, and *Av*FdI is readily apparent from the magnitude and slope of the contributions of water dipoles at small values of *r*. Thus, water dipoles at <10 Å contribute 15 to 30 kcal in *Cp*Rd, *An*hetFd, and *Av*FdI and <10 kcal in *Cv*HiPIP.

We turn now to the total Δv values. There are wide variations in Δv, from 108 kcal (*Eh*HiPIP, 1−/2− couple) to 240 kcal (*Ea*FdI). Broadly, for a given cluster similar values of $\Delta v_{Q\mu}$ lead to similar values of Δv. For the four rubredoxins, the $\Delta v_{Q\mu}$ range is 70−75 kcal and the Δv range 162−174 kcal. For the four $Fe_2S_2Cys_4$ ferredoxins, the $\Delta v_{Q\mu}$ range is 92−122 kcal and the Δv range is 228−240 kcal. For the two $Fe_3S_4Cys_3$ proteins, $\Delta v_{Q\mu}$ and Δv ranges are 84−97 and 195−211 kcal, respectively. For the 1−/2− redox couple of the $Fe_4S_4Cys_4$ proteins, the $\Delta v_{Q\mu}$ range for the four HiPIPs is 24−40 kcal and the Δv range is 108−117 kcal. In contrast, for *Av*FdI and *Bt*Fd $\Delta v_{Q\mu}/\Delta v$ are much higher: 91/144 and 68/139 kcal, respectively. For the 2−/3− couple, the $\Delta v_{Q\mu}$ range for the five low-potential ferredoxins is 68−93 kcal and the Δv range is 196−206 kcal. In contrast, for *Cv*- and *Ev*HiPIPs, $\Delta v_{Q\mu}/\Delta v$ are much lower: 36/174 and 24/172 kcal, respectively.

For a given cluster and redox couple, the variations in Δv among proteins enable variations in redox potential to be calculated. The redox potentials obtained from the PDLD calculations are given in Tables 3−9. For each cluster type and redox couple, the redox potential of one protein is chosen as a reference i.e., its calculated potential is placed equal

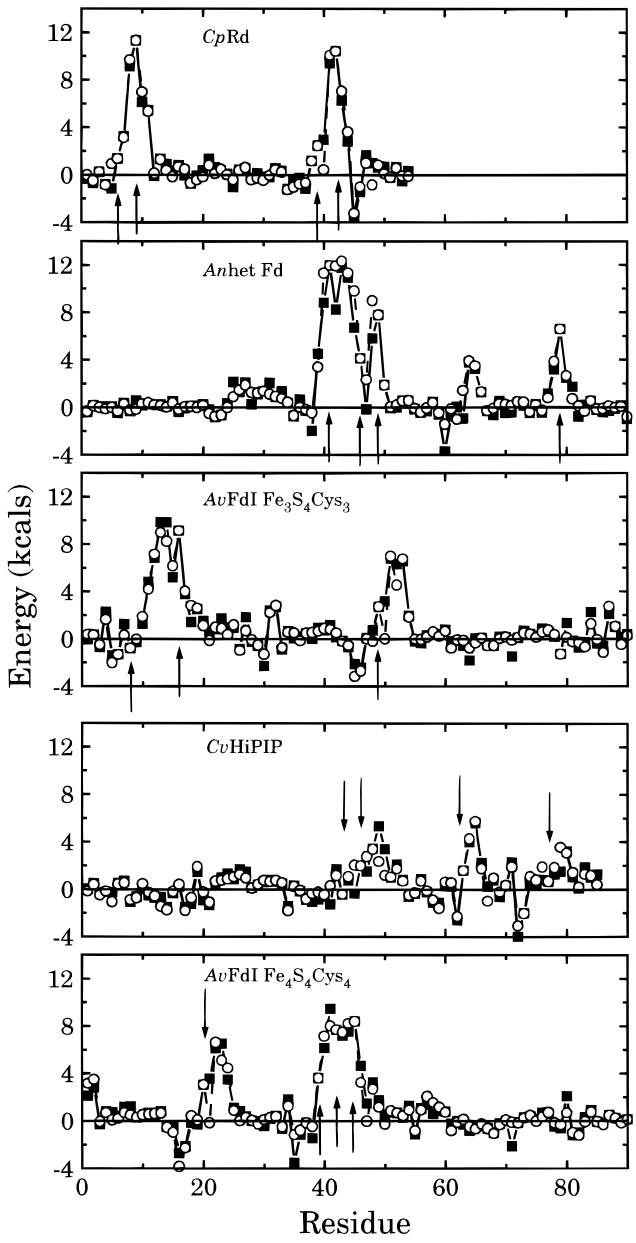

Figure 8. Δv_{Qu} resolved by amino acid residue. Δv_{Qu} resolved by total amino acid (■) and by the NH plus CO groups (○) of the polypeptide for a representative of each class of iron−sulfur cluster. The arrows indicate the positions of the Cys ligands to the cluster.

to its observed potential. The choice of protein is arbitrary.

By far the largest variations in Δv and, consequently, redox potential occur for the $Fe_4S_4Cys_4$-containing proteins. Our calculations predict the ordering of potentials for the 1−/2− couple: [*Cv*-, *Eh*-, *Ev*-, *Rt*HiPIP] ≪ [*Av*FdI, *Bt*Fd]. With *Cv*HiPIP chosen as the reference protein, the redox potentials for *Av*FdI and *Bt*Fd are predicted to be well above +1000 mV. For the 2−/3− couple, we predict [*Cv*-, *Ev*HiPIP] ≪ [*Av*FdI, *Bt*Fd, *Ca*Fd, *Da*FdI, *Pa*Fd]. With *Av*FdI chosen as the reference protein, the redox potentials for *Cv*- and *Ev*HiPIP are predicted to be well below −1000 mV. These predictions are in agreement with the inaccessibility of the 1− state for the low-potential ferredoxins and of the 3− state for the HiPIPs.[110]

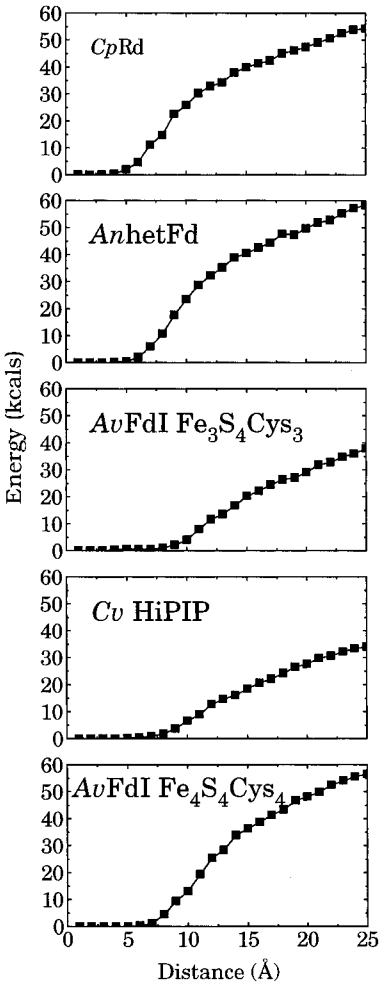

Figure 9. Radial dependence of Δv_L. Δv_L vs distance from the center of the cluster for a representative of each class of iron−sulfur cluster.

Within groups of similar proteins, the predicted variations in redox potential are less in accord with experiment. For the five rubredoxins, the predicted ordering is *Cp* < *Dd* < *Dg* < *Dv* < *Pf* in comparison to the experimental ordering of *Cp* < *Dd* ∼ *Pf* < *Dg* ∼ *Dv*. More significantly, the range of potentials predicted is 501 mV, in contrast to the observed range of 65 mV. For the four $Fe_2S_2Cys_4$ ferredoxins, the predicted order is *Sp*Fd < *An*hetFd < *An*vegFd < *Ea*FdI in comparison to the experimental ordering of *An*vegFd < *An*hetFd ∼ *Ea*FdI < *Sp*Fd. The predicted and observed ranges of potential are 507 and 60 mV, respectively. For the two $Fe_3S_4Cys_3$ ferredoxins, the predicted and experimental order are both *Av*FdI < *Dg*FdII. The predicted and observed ranges of potential are 680 and 295 mV, respectively. For the four HiPIPs, the predicted ordering is *Eh* < *Ev* < *Cv* < *Rt* in comparison to the experimental ordering of *Eh* < *Ev* < *Rt* < *Cv*. The predicted and observed ranges of potential are 384 and 240 mV respectively. For the five low-potential ferredoxins, the predicted ordering is *Da*FdI < *Pa*Fd(II) < *Bt*Fd < *Ca*Fd(I) < *Pa*Fd(I) < *Ca*Fd(II) < *Av*FdI in comparison to the experimental ordering of *Av*FdI < *Pa*Fd(I,II) < *Ca*Fd(I,II) < *Da*FdI < *Bt*Fd. The predicted and observed ranges of potential are 445 and 370 mV, respectively.

III. Molecular Dynamics

"Static" PDLD calculations ignore (1) the relaxation of the protein concomitant with the change in oxidation level of the [Fe-S] cluster; and (2) the dynamical motion of the protein which exists at ambient temperatures (where redox potentials are measured). Further, significant errors attach to the protein coordinates obtained experimentally. These errors are neither well-defined nor systematic and lead to significant uncertainties in PDLD calculations.

Molecular dynamics (MD) provides a mechanism for alleviating the deficiencies of static PDLD calculations. First, redox-dependent relaxation is introduced. Second, the dynamical motion of the real system is modeled. Third, protein structures are relaxed using a uniform protein force field, thereby compensating for the random fluctuations in experimental structures.

A. Methodology

Molecular dynamics (MD) is carried out as follows. A sphere of radius 12 Å is defined, centered on the [Fe-S] cluster. Solvent water within this sphere is modeled at the atomic level i.e. "real" water molecules are inserted. Outside, solvent water is modeled by a dipole grid inside a sphere of radius 18 Å and as continuum dielectric beyond. Atoms within the 12 Å sphere are allowed to move, while those outside are fixed. In the calculations discussed here, the Fe and S atoms of the [Fe-S] cluster are also fixed.

MD is carried out at 300 K both with the cluster in the oxidized state and with the cluster in the reduced state. Every 500 fs the structure is stored; 25 structures are generated over a total time of 12.5 ps. PDLD calculations are carried out for the 25 oxidized and 25 reduced structures. The MD-averaged Δv is then calculated using the Linear Response Approximation relationship[18,19]

$$\Delta v = {}^1/_2[\langle \Delta v \rangle_{ox} + \langle \Delta v \rangle_{red}] \qquad (12)$$

where $\langle\ \rangle_{ox}$ and $\langle\ \rangle_{red}$ denote averages over oxidized and reduced structures.

The variation in structure during MD is illustrated for *Av*FdI ($Fe_4S_4Cys_4$) in Figure 10. The variations of $\Delta v_{Q\mu}$, $\Delta v_{Q\alpha}$, Δv_L and Δv are illustrated for *Av*FdI ($Fe_4S_4Cys_4$) in Figure 11.

B. MD-PDLD Calculations

The results of MD-PDLD calculations are given in Tables 3−9 and Figures 2−7.

$FeCys_4$ Proteins. The changes in Δv due to MD are in the range −6 to +6 kcal; the largest are for *Cp*Fd (+6) and *Pf*Rd (−6). The range of Δv values is substantially reduced and is now 168−172 kcal. Consequently, the range of predicted redox potentials is reduced to 163 mV from 501 mV. When compared to the experimental range, 65 mV, this is a major improvement. The predicted redox potential order is now *Cp* < *Pf* < *Dg* < *Dd* < *Dv* compared to the experimental order *Cp* < *Dd* ∼ *Pf* < *Dg* ∼ *Dv*. Given the narrowness of the range of observed potentials the significance of comparing the predicted and observed orderings of potentials is not great.

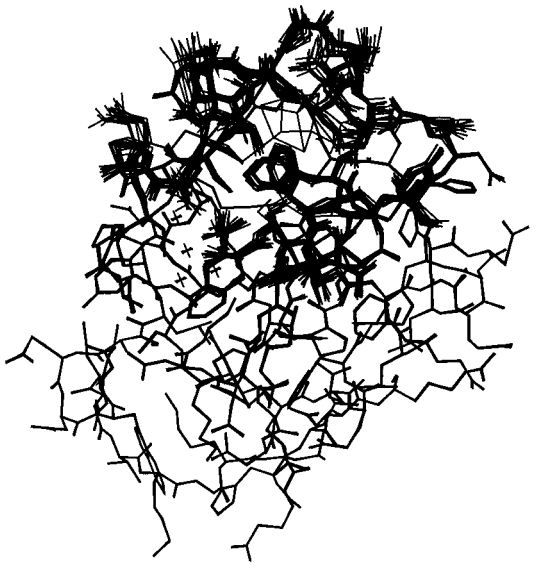

Figure 10. Molecular motion during molecular dynamics. Superposition of 12 structures obtained at 1 ps intervals during molecular dynamics on *Av*FdI. The region outside 12 Å from the center of the cluster and the cluster itself are constrained to the crystallographic coordinates.

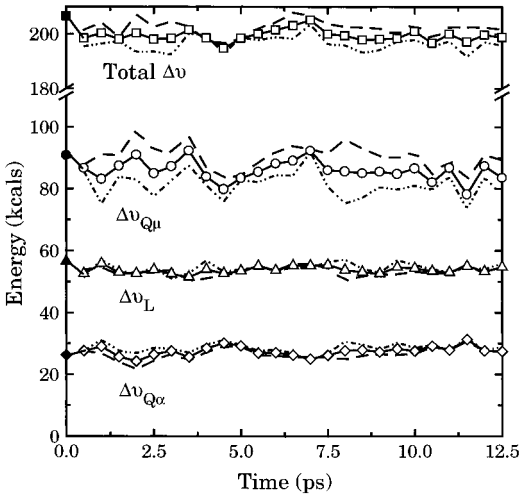

Figure 11. Time dependence of PDLD energies during molecular dynamics. Δv and its components ($\Delta v_{Q\mu}$, $\Delta v_{Q\alpha}$, and Δv_L) during MD with the cluster in the oxidized state (- · · -) and the reduced state (- - -) are shown. The open symbols represent an average of these energies and the closed symbols are the energies obtained on the initial crystal structure.

$Fe_2S_2Cys_2$ Proteins. The changes in Δv due to MD are in the range −5 to +10 kcal; for the four proteins, the largest are for *An*vegFd (−5) and *Sp*Fd (+10). The range of Δv values is substantially reduced and is now 233−239 kcal. Consequently, the range of predicted potentials is reduced to 248 mV from 507 mV. When compared to the experimental range, 60 mV, this is a substantial improvement. The predicted redox potential order is now *An*vegFd < *Ea*FdI < *Sp*Fd < *An*hetFd compared to the experimental ordering of *An*vegFd < *An*hetFd ∼ *Ea*FdI < *Sp*Fd.

$Fe_3S_4Cys_3$ Proteins. The changes in Δv due to MD are 0 and 8 kcal for *Av*FdI and *Dg*FdII, respectively, substantially changing the difference in Δv from 16 to 7 kcal. This corresponds to a change in the difference of these potentials from 680 mV to 319

Table 10. RMS Deviations for PDLD and MD-PDLD Calculations

	Δ^a (mV)	minimum rms^b (mV)
$FeCys_4^{1-/2-}$		
PDLD	−240	78
MD-PDLD	10	26
$Fe_2S_2Cys_4^{2-/3-}$		
PDLD	−20	103
MD-PDLD	80	40
$Fe_3S_4Cys_3^{2-/3-}$		
PDLD	−190	136
MD-PDLD	−10	8
$Fe_4S_4Cys_4^{1-/2-}$		
PDLD	−40	35
MD-PDLD	−50	34
$Fe_4S_4Cys_4^{2-/3-}$		
PDLD	260	70
MD-PDLD	120	30
AvFdI mutants		
PDLD		41^c
MD-PDLD		22^c

^{a} Change in potential to obtain minimum rms relative to results shown in Tables 3−7. ^{b} Rms deviation from observed potentials at the optimum Δ. ^{c} Rms determined with the potential of native *Av*FdI set to −650 mV.

mV. In comparison to the experimental difference of 295 mV, agreement is substantially improved.

$Fe_4S_4Cys_4$ Proteins. For the 1−/2− couple of the four HiPIPs, the changes in Δv due to MD are very similar and ∼−9 kcal. The range of Δv values is thus essentially unaltered and is now 99 to 108 kcal. Consequently, the range of predicted potentials is also very similar: 371 mV as compared to 384 mV. The agreement with the experimental range, 240 mV, is not changed. The predicted redox potential order is still *Eh* < *Ev* < *Cv* < *Rt*.

For the 2−/3− couple of the five low-potential ferredoxins, the changes in Δv due to MD are in the range −7 to +4 kcal; the largest is for *Av*FdI (−7). The range of Δv values is now 199 to 207 kcal, very little different from the 196−206 kcal range before MD. The range of predicted redox potentials is changed to 324 mV from 445 mV, to be compared to the experimental range of 370 mV. The predicted redox potential order is now *Pa*Fd(II) < *Av*FdI < *Da*FdI < *Ca*Fd(I) < *Ca*Fd(II) < *Pa*Fd(I) < *Bt*Fd compared to the experimental order *Av*FdI < *Pa*Fd-(I,II) < *Ca*Fd(I,II) < *Da*FdI < *Bt*Fd. The predicted order is in substantially improved agreement with experiment.

The predicted variations in potential of the 1−/2− couple for *Cv*HiPIP, *Av*FdI, and *Bt*Fd and of the 2−/3− couple for *Av*FdI, *Cv*HiPIP, and *Ev*HiPIP are modified by MD. However, the conclusion that for each couple, the potentials of the low-potential ferredoxins are enormously higher than those of the HiPIPs are unaffected.

An overview of the accuracy of the PDLD and MD-PDLD calculations in reproducing variations in experimental redox potentials is provided by Table 10 and Figure 12. For each set of proteins we have varied the intrinsic redox free energy to yield a minimum RMS deviation of calculated and experimental redox potentials. The RMS deviations so obtained are listed in Table 10. The corresponding calculated redox potentials are compared to experimental redox potentials in Figure 12. The RMS deviations are in the range 35 to 136 mV for the PDLD calculations and in the range of 8 to 40 mV for the MD-PDLD calculations. The MD-PDLD calculations are superior to the PDLD calculations for every category of protein. This improvement is clearly demonstrated in Figure 12.

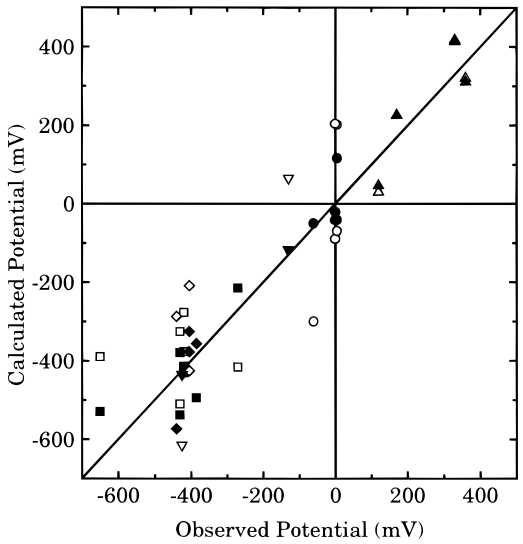

Figure 12. Comparison of calculated redox potentials to the observed. Minimum RMS best fit between calculated and observed redox potentials are shown for: $FeCys_4$ (•); $Fe_2S_2Cys_4$ (◆); $Fe_3S_4Cys_3$ (▼); $Fe_4S_4Cys_4^{1-/2-}$ (▲); $Fe_4S_4Cys_4^{2-/3-}$ (■). The open symbols represent the redox potentials obtained from PDLD calculations and the closed symbols represent those obtained from MD-PDLD calculations. The diagonal line shows ideal agreement.

IV. Mutants

Many mutant [Fe-S] proteins have by now been obtained via site-directed mutagenesis and studied. To date, structures have been only reported for mutants of *Av*FdI. Table 2 lists those *Av*FdI mutants whose structures have been determined, together with their PDB file names. All structures were obtained via X-ray crystallography; Table 2 lists the resolutions of the diffraction data. Redox potentials have in all cases been measured and, for the 2−/3− $Fe_4S_4Cys_4$ cluster, are also listed in Table 2.[111]

For all but two of the *Av*FdI mutants the ligations of the two clusters are unchanged from the native protein. In two mutants: C20A and C20S, C24 replaces C20 as the fourth Cys ligand of the $Fe_4S_4Cys_4$ cluster.

The results of PDLD and MD-PDLD calculations on five mutants of *Av*FdI for the 2−/3− couple of the $Fe_4S_4Cys_4$ cluster are given in Table 11 and Figure 13. The PDLD calculations predict an ordering of potentials: C20S < C20A < F25I < native < C24A < F2Y compared to the experimental ordering C20A < C20S < F25I < native ∼ F2Y < C24A. The calculated and experimental ranges are 194 and 150 mV, respectively. The MD-PDLD calculations predict an ordering of C20A < C20S < F25I < native < F2Y < C24A with a range of 297 mV. The ordering and range are in better and worse agreement with experiment, respectively.

Table 11. Mutants of *Av*FdI

	*Av*FdI		F2Y		C20A		C20S		C24A		F25I	
	PDLD	MD-PDLD	PDLD	MD-PDLD	PDLD	MD-PDLD	PDLD	MD-PDLD	PDLD	MD-PDLD	PDLD	MD-PDLD
$\Delta v_{Q\mu}$	90.82	85.97	94.03	88.99	86.83	78.02	83.76	79.46	89.06	88.61	92.26	86.44
$\Delta v_{Q\alpha}$	26.17	27.48	25.63	26.69	30.36	32.78	32.42	32.1	27.05	26.71	24.18	25.66
Δv_L	56.46	53.79	55.29	52.34	53.65	51.9	55.11	53.15	57.83	53.49	56.2	54.9
Δv_B	32.98	32.23	32.92	32.26	32.75	31.73	32.09	32.21	33.05	32.46	33.1	31.99
Δv	206.43	199.47	207.87	200.27	203.59	194.43	203.38	196.91	206.99	201.27	205.74	198.98
$\Delta\Delta v$	0	0	1.44	0.8	−2.84	−5.04	−3.05	−2.56	0.56	1.8	−0.69	−0.49
ϵ_{calc}[a]	−650	−650	−588	−615	−773	−869	−782	−761	−626	−572	−680	−671
ϵ_{obs}	−650		−650		−750		−690		−600		−670	

[a] Native *Av*FdI is chosen as the reference protein.

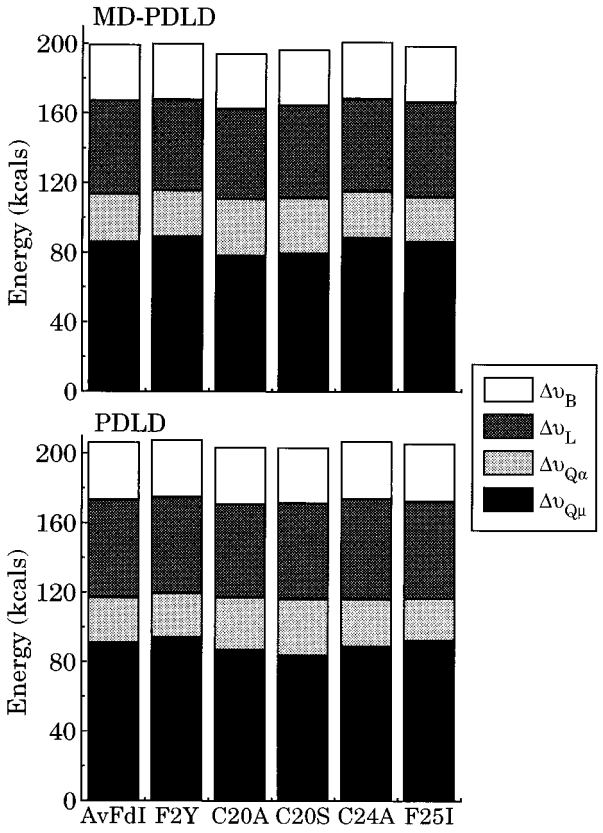

Figure 13. PDLD calculations for site directed mutants of *Av*FdI. Components of Δv are calculated with (MD-PDLD) and without (PDLD) molecular dynamics averaging.

RMS deviations of calculated and experimental variations in potential are given in Table 10. On average, the MD-PDLD calculations are more accurate.

V. Charged Residues

In the PDLD calculations described above the total charge of the protein is equal to the charge on the [Fe-S] cluster. All acidic and basic residues are in their uncharged form. In practice, all [Fe-S] proteins contain residues which are charged at the pH values where redox potentials are measured. (Typically, acidic residues preponderate in [Fe-S] proteins.) In neglecting the charges of such residues, our PDLD calculations are incomplete.

The accurate calculation of the effects of charging residues on [Fe-S] redox potentials is difficult. Protonation or deprotonation of a residue is accompanied by deprotonation or protonation of the protein or solvent (which is, of course, always buffered) and the effects of the latter are equally important and must be included simultaneously. This is not easy to model microscopically. Accordingly, at the present time we elect to treat the contributions of the charges of charged residues macroscopically. That is, the interaction of the charge of a residue with cluster charges is modulated by a dielectric constant.

Table 12. Number of Ionizable Residues and Total Charges of [Fe-S] Proteins

cluster type	protein	total[a] charge	ionizable residues				
			Asp	Glu	His	Lys	Arg
$FeCys_4$	*Cp*Rd	−12	10	6	0	4	0
	*Dd*Rd	−5	6	2	1	2	0
	*Dg*Rd	−6	8	3	0	5	0
	*Dv*Rd	−6	6	4	0	4	0
	*Pf*Rd	−8	7	6	0	5	0
$Fe_2S_2Cys_4$	*An*hetFd	−9	8	10	2	5	2
	*An*vegFd	−14	11	10	2	4	1
	*As*FdI	−14	12	8	1	4	1
	*Ea*FdI	−14	7	13	1	4	1
	*Sp*Fd	−16	12	8	1	2	1
$Fe_3S_4Cys_3$	*Av*FdI	−16	11	14	2	6	1
	*Dg*FdII	−15	8	9	0	1	1
$Fe_4S_4Cys_4^{1-/2-}$	*Cv*HiPIP	−1	5	4	1	5	2
	*Eh*HiPIP	−7	7	8	4	1	3
	*Ev*HiPIP	−4	5	5	2	1	3
	*Rt*HiPIP	5	3	0	0	7	1
$Fe_4S_4Cys_4^{2-/3-}$	*Av*FdI	−16	11	14	2	6	1
	*Bt*Fd	−17	15	6	0	4	0
	*Ca*Fd[b]	−8	6	3	0	0	1
	*Da*FdI	−13	6	12	1	3	1
	*Pa*Fd	−7	5	3	0	1	0

[a] All Asp and Glu are 1−, all His, Lys and Arg are 1+. [b] Based on the sequence in ref 57.

In Tables 3−7 we give estimates of the contributions of the charges of charged residues to the redox free energy for the [Fe-S] proteins discussed above. The numbers of residues which can be charged in each protein are listed in Table 12. The contributions are labeled Δv_{QQ} and are obtained as follows. All residues which can be charged in a given protein are protonated or deprotonated, as appropriate, and the net (+) and (−) charges resulting distributed over the basic or acidic groups. Δv_{QQ} is the resulting change in $\Delta v_{Q\mu}$, divided by the dielectric constant, ϵ. In Tables 3−7 we use $\epsilon = 80$.

The values of Δv_{QQ} are almost always negative (*Cv*HiPIP and *Rt*HiPIP are the only exceptions) as expected for proteins in which acidic residues generally predominate. Magnitudes lie in the range 0−5 kcal. Variations in Δv_{QQ} with protein yield contributions to redox potential differences which are almost

Table 13. Change in Potential Due to Change in Charged Residues in Mutants of *Av*FdI

	native[a]	D23N	H35D	E38S	E46A
Δv_{QQ}	−4.74	−4.27	−5.44	−4.36	−4.34
$\Delta\Delta v_{QQ}$	0	0.47	−0.7	0.38	0.4
$\Delta\epsilon_{calc}$	0	20	−30	16	17
$\Delta\epsilon_{obs}$		0	0	0	0

[a] Reference protein.

always in the range 0−100 mV. Thus, these calculations lead to the general conclusion that the charges of charged residues can contribute to variations in redox potential on the tens of millivolt scale, but are unlikely to be responsible for variations on the hundreds of millivolt scale.

Experimental studies of a number of mutants of *Av*FdI in which the number of charged residues is changed permit the simple methodology adopted above to be tested. The X-ray structures and Fe_4S_4-Cys_4 redox potentials of the D23N, H35D, E38S, and E46A mutants have been determined (Table 2). Residues 23, 35, 38, and 46 are all surface residues in the neighborhood of the $Fe_4S_4Cys_4$ cluster. In these mutant proteins, the redox potentials of the $Fe_4S_4Cys_4$ clusters were in every case identical to that in the native protein (under the same experimental conditions, of course). That is, none of these mutations produced a detectable shift in redox potential. Values of Δv_{QQ} for the four mutant proteins are given in Table 13. With $\epsilon = 80$, changes of 20, −30, 16, and 17 mV are predicted for D23N, H35D, E38S, and E45A, respectively. These predicted changes are much larger than the experimental changes, 0 mV. It follows that for these specific charged residues, the appropriate value of ϵ is much larger than 80.

If ϵ is much larger than 80 for all charged residues in [Fe-S] proteins, the Δv_{QQ} values given in Tables 3−7 are substantially too large and the contributions of charged residues to variations in potential are even less important than was indicated. Alternatively, it is possible that the assumption of a single dielectric constant for all residues is incorrect and that the protein should be treated as an *in*homogeneous dielectric, when the contributions of charged residues at different locations in the protein require different dielectric constants. This idea is not new.[14]

At this time, it is reasonable to conclude that large variations (hundreds of millivolt) in potential between proteins are very unlikely to originate predominantly in differences in the contributions of ionized residues. Small contributions are probable but simple macroscopic electrostatic calculations using a single, uniform dielectric constant are insufficiently reliable to provide reliable predictions of their magnitude.

VI. Predictions

We have carried out calculations for two proteins whose structures have been determined but for which redox potentials are not available: *As*FdI and *Ec*EnIII.

*As*FdI is a typical algal $Fe_2S_2Cys_4$ ferredoxin. Its structure is quite similar to those of *An*HetFd, *An*vegFd, *Ea*FdI, and *Sp*Fd.[35−39] Its redox potential does not appear to have been reported. The results of MD-PDLD calculations are given in Table 4 and Figure 3. The potential of *As*FdI is predicted to be equal to *An*hetFd, and greater than *An*vegFd, *Ea*FdI, and *Sp*Fd. Our calculations confirm the intuitive expectation that the potential of *As*FdI will be typical of plant and algal ferredoxins i.e. ∼ −350 to −450 mV.[82]

*Ec*EnIII, by contrast, is a unique protein. Its Fe_4S_4-Cys_4 cluster is ligated by the unprecedented Cys-X_6-Cys-X_2-Cys-X_5-Cys sequence.[72] As isolated, its cluster is in the 2− state.[112] Neither reversible oxidation nor reduction have been unambiguously observed. Reduction to the 3− state at very low potential was reported by Cunningham et al.;[111] more recently, however, Fu et al.[104] have attributed the previously observed 3− EPR to O_2-damaged protein. Oxidation with $Fe(CN)_6^{3-}$ has been reported to lead to formation of a $Fe_3S_4Cys_3$ cluster.[111] The folding of the polypeptide of *Ec*EnIII around its $Fe_4S_4Cys_4$ cluster is quite different from that in any other [Fe-S] protein. In particular, it bears no obvious resemblance to either the HiPIPs or the low-potential ferredoxins. The redox potentials of its cluster can therefore not be anticipated by analogy. In this situation, molecular modeling is clearly a useful guide. The results of MD-PDLD calculations on *Ec*EnIII for the 1−/2− and 2−/3− couples of the $Fe_4S_4Cys_4$ cluster are given in Tables 8 and 9, respectively, and in Figure 7. The potential of the 1−/2− couple is predicted to be comparable to that of *Cv*HiPIP; the potential of the 2−/3− couple is predicted to be > 1000 mV lower than that of *Av*FdI. Thus, our calculations firmly place *Ec*EnIII with the HiPIPs and suggest that (i) under suitable conditions, its 1−/2− couple may be observable while (ii) its 2−/3− couple is likely to be inaccessible. Experiments are underway to evaluate these conclusions.

VII. Prior Literature

A variety of factors have been proposed to contribute to variations in the redox potentials of [Fe-S] clusters with protein environment, including (i) hydrogen bonding, (ii) solvent accessibility, and (iii) charges on acidic and basic residues.

Hydrogen Bonding. Following the solution of the X-ray structures of *Pa*Fd and *Cv*HiPIP in the early 1970s[27] it was proposed that the differences in the redox potentials of the 1−/2− and 2−/3− couples of their structurally indistinguishable $Fe_4S_4Cys_4$ clusters resulting in the former couple being expressed in *Cv*HiPIP and the latter in *Pa*Fd could be attributed principally to the differences in protein−cluster hydrogen (H)-bonding.[110] In each cluster of *Pa*Fd, eight amide N−H-to-cluster S (S* or Cys Sγ) H-bonds were identified on the basis of N···S distances. In the case of *Cv*HiPIP, five such H-bonds were found. N−H···S H-bonding would be expected to increase with increasing cluster negative charge. Increased H-bonding would therefore be expected to raise both 1−/2− and 2−/3− redox potentials. It was postulated that the greater H-bonding in *Pa*Fd compared to *Cv*HiPIP makes accessible the 2−/3− couple, but not the 1−/2− couple, in the former and vice versa in the latter.

Table 14. N−H···S H-Bond Contributions to $\Delta v_{Q\mu}$

	*Cp*Rd			*An*hetFd			*Av*FdI $Fe_3S_4Cys_3$			*Cv*HiPIP			*Av*FdI $Fe_4S_4Cys_4$		
	res[a]	N−S[b]	$\Delta v_{Q\mu}$[c]	res	N−S	$\Delta v_{Q\mu}$	res	N−S	$\Delta v_{Q\mu}$	res	N−S	$\Delta v_{Q\mu}$	res	N−S	$\Delta v_{Q\mu}$
	8	3.67	3.62	43	3.18	6.62	13[d]	3.59	3.96	48	3.68	2.31	2	3.4	3.58
	9	3.67	5.42	44	3.64	5.74	14	3.15	4.65	65	3.52	3.63	22[e]	3.64	3.94
	11	3.47	6.1	45	3.39	4.42	15[d]	3.48	1.85	77	3.66	1.22	24[e]	3.57	3.73
	41	3.58	4.38	48	3.39	3.82	16	3.43	4.77	79	3.47	2.86	40	3.46	3.58
	42	3.61	6.02	79	3.58	5.74	32[d]	3.56	3.75	81	3.68	3.14	41	3.3	3.44
	44	3.84	5.54				51	3.37	4.19				43	3.22	3.3
							53	3.3	4.41				44	3.42	3.69
													45[e]	3.7	4.41
$\Delta v_{Q\mu}$ of NH groups			31.08			26.34			27.58			13.16			29.67
total $\Delta v_{Q\mu}$			70.36			114.07			96.79			35.84			90.82
% in H-bonds			44			23			28			37			33

[a] Residue containing the H-bonding N-H group. [b] Distance from N to the closest cluster S (Å). [c] Energy (kcal) contributed to $\Delta v_{Q\mu}$ by the NH group. [d] Defined as N−H···S H-bonds by Merritt et al. (ref 44) but not by Stout (ref 45). [e] Defined as N−H···S H-bonds by Backes et al. (ref 60), but not by Merritt et al. (ref 44) and Stout (ref 45).

Subsequent X-ray structural data have not supported the hypothesis of a simple, general relationship between cluster−protein H-bonding and redox potential. In the case of the rubredoxins, *Cp*, *Dd*, *Dg*, *Dv*, and *Pf*, there is great similarity between the $FeCys_4$ environments; in particular, six H-bonds are conserved.[28−32] The redox potentials of these proteins vary very little. In contrast, in the case of the HiPIPs of *Cv*, *Eh*, *Ev*, and *Rt* there is also great similarity in the $Fe_4S_4Cys_4$ cluster environments; in particular, five H-bonds are conserved.[50−53] However, their redox potentials vary by more than 200 mV. Likewise, in the case of the low-potential ferredoxins of *Av*, *Bt*, *Ca*, *Da*, and *Pa*, there is great similarity in the cluster environments; in particular, eight H-bonds are conserved.[44,45,56−60] However, their redox potentials vary by nearly 400 mV. The situation is less simple in the case of the $Fe_2S_2Cys_4$ and $Fe_3S_4Cys_3$ ferredoxins. In the former, there is considerable similarity in the environments of the $Fe_2S_2Cys_4$ clusters in *An*het, *An*veg, *Ea*, and *Sp* ferredoxins, and, in particular, in their H-bonding.[35,36,38,39] However, the reported H-bonding does vary, both with respect to the number of H-bonds and their heterogeneity (in some proteins, but not others, O−H···S H-bonds also being reported). The redox potentials vary less than 100 mV. In the case of the $Fe_3S_4Cys_3$ clusters of *Av*FdI and *Dg*FdII, four[45] or seven[44] and eight[47] H-bonds were reported respectively. Their redox potentials differ by ∼300 mV.

In sum: at this time, there is clearly not a simple correlation between H-bonding and redox potential. The identification of cluster−protein H-bonds depends of course on (i) the criteria (e.g. N···S distance) used to identify H-bonds and (ii) the accuracy of the structural coordinates. Different crystallographers have used different criteria: the relative numbers of H-bonds reported can change significantly if the criteria are changed. (For example, the different numbers of H-bonds reported for the *Av*FdI and *Dg*FdII $Fe_3S_4Cys_3$ clusters[44,45,47] in part reflect different N···S distance criteria.) In addition, some structures are less accurate than others and changes can be expected with further refinement. Nevertheless, it is extremely unlikely that future comparisons of H-bonding will cause a simple correlation with redox potential to emerge.

It is possible that H-bonding is a major factor, but that variations in other factors must be included to obtain the experimentally observed variation in redox potential. Alternatively, it is possible that H-bonding is not a major factor. The PDLD calculations presented above make clear the necessity of including all major contributions to redox potential variations and so the former position cannot be immediately eliminated. However, at the same time our calculations do lead to the conclusion that H-bonding is not a dominant factor. The PDLD calculations model the interactions of H-bonding X−H groups with clusters via the contributions of these groups to $v_{Q\mu}$. That is, H-bonding is modeled electrostatically. The magnitudes of the contributions to $\Delta v_{Q\mu}$ of N−H groups identified as H-bonding in a selection of proteins are listed in Table 14, together with the total $\Delta v_{Q\mu}$, values. It is clear that the H-bonding contributions are less than 50% of the total $\Delta v_{Q\mu}$. This is to be expected; (i) many more amide groups contribute significantly to $\Delta v_{Q\mu}$ than are located within H-bonding distances; and (ii) the contributions of the C═O amide moiety are comparable to those of the N−H moiety, but are omitted when only H-bonding interactions are included. It is clear that to focus exclusively on H-bonding N−H groups is to ignore the majority of the electrostatic interaction of the cluster with the protein.

Obviously, a purely electrostatic model of H-bonding is inexact and our modeling of cluster−protein H-bonding can be improved. However, it is extremely unlikely that a more sophisticated treatment of H-bonding will significantly change our general conclusion.

Solvent Accessibility. The redox potentials of proteins in solution are dependent on the nature of the solvent. Further, for proteins in a given solvent—for example, water—redox potentials must depend on the proximity of the redox active prosthetic group and solvent. This in turn is a function of (i) the size of the protein, (ii) the location of the prosthetic group within the protein, and (iii) the extent to which solvent molecules are intercalated within the protein.

Many authors have recognized the importance of the solvent in determining the redox potentials of [Fe-S] proteins. The term "solvent accessibility" is frequently used, and redox potentials are expected

to become increasingly positive with increasing solvent accessibility. Thus, for example, clusters very near the surface of a protein exhibit higher solvent accessibility than those buried in the interior and the redox potentials of the former should be elevated accordingly. In the smaller [Fe-S] proteins, clusters are in all cases close to the protein surface with the exception of the $Fe_4S_4Cys_4$ clusters of the HiPIPs, which are more centrally located within the proteins. It has been proposed that lower solvent accessibility of HiPIP clusters compared to those of low-potential ferredoxins contributes to the lower potentials (for a given redox couple) of the HiPIPs.

In the case of groups of proteins of similar size and structure, the relative solvent accessibilities of clusters in different proteins is much harder to evaluate. When X-ray structures are available there are two approaches commonly adopted. First, the proximity of a cluster to the protein surface can be quantitated by such procedures as rolling a sphere along the surface to find the position of closest approach. Second, the solvent model generated during X-ray structure refinement can be analyzed. In general, physically meaningful solvent models require fairly high resolution X-ray data. In the case of the [Fe-S] proteins, most attention has been paid to the solvent models of the rubredoxins as a result of the relatively high resolutions of their diffraction data. Overall, the quality of the solvent models varies widely.

To date, there is no pair (or set) of proteins containing the same cluster and exhibiting the same redox couple whose redox potential differences can be clearly correlated with an objective measure of solvent accessibility. Probably the most careful examination of this topic is the comparison of *Av*FdI and *Pa*Fd by Merritt et al.[44] Since the $Fe_4S_4Cys_4$ clusters of these proteins possess very similar protein environments—including homologous H-bonding—it has been hypothesized that the 230 mV redox potential difference originates in greater solvent accessibility of the clusters of *Pa*Fd.[60] Unfortunately, careful comparison of the *Av*FdI and *Pa*Fd structures could not find evidence supporting this hypothesis.

Our PDLD calculations confirm the importance of the solvent in modulating [Fe-S] protein redox potentials. The Δv_L terms are substantial and generally comparable in magnitude to $\Delta v_{Q\mu}$ and $\Delta v_{Q\alpha}$. The variations in Δv_L contribute importantly to the net variations in Δv. In addition, our calculations permit the interrelationship of the solvent contribution and the protein structure to be analyzed. A number of general conclusions are clear. First, the magnitude of Δv_L decreases with increasing protein size—simply due to the decreasing space accessible to solvent. However, this does not automatically lead to decreasing redox potentials because the decrease in Δv_L is compensated by the increasing magnitude of $\Delta v_{Q\mu}$ and $\Delta v_{Q\alpha}$. There is therefore *not* a simple connection between protein size and redox potential. Second, the magnitude of Δv_L is a function of the charge distribution of the protein as well as of its spatial distribution; all other things being equal, increases in $\Delta v_{Q\mu}$ generally lead to decreases in Δv_L. Thirdly, local solvent environments do not generally dominate the variations in Δv_L. That is, in general the differences in Δv_L between two proteins is not well-represented by the differences in contributions of solvent close to the cluster (e.g. within 10 Å). Fourthly, intercalated water can contribute significantly to Δv_L.[9]

The solvent model adopted in PDLD calculations is microscopic, but not atomic. The former permits the contributions of intercalated water to be modeled, in contrast to macroscopic continuum dielectric models. However, the latter inhibits detailed comparison of the solvent model with those obtained via X-ray crystallography. Clearly, future calculations should increasingly incorporate atomistic—and, therefore, more realistic—treatments of the solvent, permitting such comparison to take place. At the same time, X-ray structures can be expected to be refined to higher resolutions providing increasingly reliable solvent models. Ultimately, solvent models used in calculations of redox potentials must be consistent with the average solvent structure obtained from X-ray crystallography.

Charged Residues. Variations in the number of charged residues have frequently been invoked to rationalize variations in redox potentials among [Fe-S] proteins. For example, the more negative charges of the *Eh*- and *Ev*HiPIPs relative to *Cv*HiPIP (see Table 12) have been correlated with their substantially lower redox potentials.[51,52] However, when a larger number of proteins are examined, such correlations are not sustained. For the proteins listed in Table 12, the total charges vary by 7, 7, 1, 12, and 10 for the $FeCys_4$, $Fe_2S_2Cys_4$, $Fe_3S_4Cys_3$, $Fe_4S_4Cys_4$ (1−/2−), and $Fe_4S_4Cys_4$ (2−/3−) proteins respectively; the variations in redox potential are 65, 60, 295, 240, and 270 mV. For a given [Fe-S] cluster and redox couple, the experimental potentials do not vary monotonically with the protein charges. The lack of correlation is not surprising. The contribution of a specific charged residue must vary inversely with its distance from the cluster and a simple counting of charges without consideration of their locations is obviously unphysical.

Variations in redox potential with pH originate in changes in the charges of residues which can be protonated or deprotonated. For example, the potential of *Cv*HiPIP increases by ~35 mV from pH 7 to pH 4 due to protonation of its one histidine residue. Heering et al. use this change in potential together with a distance from the $Fe_4S_4Cys_4$ cluster of 8.5 Å to deduce a dielectric constant of 48 for the interaction of the charged His with the cluster.[91] In contrast, in *Ev*HiPIP, which possesses two histidines, the potential is pH independent over the range 4−11,[91] indicating a very much larger dielectric constant. The histidines of *Cv*HiPIP and *Ev*HiPIP are in different locations relative to the cluster and to the protein surface. These results support the expectation that charged residues at different distances from an [Fe-S] cluster and in different environments require different dielectric constants to predict their contributions to redox potentials. However, even for histidines the generality of this conclusion is unclear. Histidines are relatively uncommon in [Fe-S] proteins and [Fe-S] proteins are generally difficult to study at acidic pH. As a result, there is a paucity of

experimental data. In addition, not all experimental data are consistent. Different studies of the pH dependence of the redox potentials of HiPIPs have obtained significantly different results.[91,113]

It is clear that the charges of charged residues can contribute significantly to [Fe-S] cluster redox potentials. The problem is to predict the magnitude of the effect. There is a need for a much larger quantity of experimental data on the changes of potential caused by changes in residue charge resulting from either change in pH or change in amino acid side chain (chemical modification or mutagenesis).

VIII. Discussion

The theory of the redox potentials of metalloproteins is a branch of the general theory of the thermodynamics of ionic solutions. In the case of very simple ionic solutions, theoretical understanding is well advanced. In the case of solutions of complex macromolecules, such as proteins, theory is (not surprisingly) much less developed. The purpose of the studies reviewed here is to apply state-of-the-art theory to a class of proteins—specifically, [Fe-S] proteins—and to evaluate the extent to which it permits their redox potentials to be successfully predicted. To the extent that theory accounts for the observed variations in redox potential, it affords a reliable basis for interpreting their origins. To the extent that theory fails, our results provide a stimulus to develop improved theoretical methodologies.

The most important conclusion of our work is that in modeling the variations of redox potential with protein environment it is essential to include the Coulombic interaction of the charged cluster with the entire protein, to allow for the polarizability of the protein, and to include the interaction of both the cluster and the protein with the aqueous solvent bath. If any one of these phenomena is omitted, the results will be wildly inaccurate. Our model is the first to simultaneously and quantitatively include all three phenomena in discussing the redox potentials of [Fe-S] proteins.

How good is the current model? At the present stage of testing, the average accuracy of predicted redox potential variations appears to be better than 50 mV (Table 10). However, this result is quite tentative, since it is based on extremely limited statistics. The numbers of proteins containing a specific cluster type whose structures are known is very small. Further, the heterogeneity of protein structures varies widely. In the case of the rubredoxins, the $Fe_2S_2Cys_4$ ferredoxins and the HiPIPs the proteins selected for study vary (in size, sequence, homology) much less than in the case of the low potential $Fe_4S_4Cys_4$ ferredoxins. A much wider diversity of structures, as well as a much larger absolute number, will be needed to reliably define the accuracy of our model.

To some extent, errors in our predictions are likely to reflect deficiencies in the structures available. The resolutions of the X-ray structures we have used vary widely—from 1.0 to 2.5 Å—and it is likely that the poorer resolution structures will change significantly if further studied at higher resolution. Clearly, the continually increasing resolution of protein crystal structures will greatly benefit future studies of structure−redox potential relationships. However, even when accurate X-ray structures are available, there is always the possibility that the crystal and solution structures differ. Where possible, it is clearly important to compare the results obtained from X-ray crystal and NMR solution structures. To date, few NMR structures of [Fe-S] proteins have been determined (see Table 2). Undoubtedly, this will change in the relatively near future.

Errors in predicted redox potential variations also reflect the limitations of the model. The most serious deficiencies of the PDLD model are associated with the simplified treatment of the aqueous solvent and of charged residues. The advantage of the Langevin dipole model is that it not only incorporates bulk water but also intercalated water, i.e. water *inside* the protein. Its disadvantage is that it does not do this at the atomic level, i.e. it does not use real water molecules. Some of the errors in predicted redox potentials probably originate in inaccurate modeling of intercalated water. This is remediable. The incorporation of atomic water, at least for intercalated water and for surface water layers, is practicable at this time. Future studies will improve the model in this manner. The treatment of charged residues can also be improved. First, the pK, and hence the charge, of each residue at a given pH can be more accurately predicted. Second, the extra contribution of the charge on the charged residue can be calculated more accurately. In the calculations reported here, a uniform macroscopic dielectric constant has been used in scaling the Coulombic interaction of charged residues with the cluster. This approximation can be improved either by using variable dielectric constants or, better, by calculating the interaction microscopically, i.e. without a macroscopic dielectric constant.

It is also important to improve the MD averaging of PDLD calculations. We have shown that MD averaging substantially improves the accuracy of PDLD calculations. MD is a reflection of the force field employed. We can expect that improvements in the force field will lead to more accurate predictions of redox potentials.

What are the implications of our results for biochemistry? First, it is clear that proteins can tune the potential of a given redox couple of a given cluster over a very wide range—thousands, not just tens or hundreds of millivolts. The interaction energies of clusters with their environments are on the order of 100 kcal; 1000 mV variations require only 23 kcal variations in energy. Our calculations show that variations of this magnitude are easily accomplished. For the proteins we have studied the most dramatic variations occur for the $Fe_4S_4Cys_4$ proteins where changes of nearly 100 kcal occur between HiPIPs and low-potential ferredoxins. The variations for other clusters are smaller. However, this simply reflects the more limited diversity of protein environments sampled by those proteins of known structure. It can be confidently predicted that $FeCys_4$, $Fe_2S_2Cys_4$, and $Fe_3S_4Cys_4$ proteins whose redox potentials span ranges of 1000 mV and more can be constructed.

Whether variations of this magnitude occur in Nature or will only be expressed in unnatural, synthetic proteins remains to be established, of course. It is possible that for physiological, rather than chemical, reasons only more limited ranges are biologically useful. However, at this time it is reasonable to expect that as new and increasingly diverse [Fe-S] proteins are discovered, the ranges of known redox potentials will grow dramatically.

A further, corollary conclusion is that when a new protein is identified with an unconventional redox potential, it should not be automatically assumed that the unusual potential reflects a change in cluster ligation. In the case of $Fe_2S_2Cys_4$ proteins, it has been known for many years that "Rieske proteins" contain Fe-S clusters very similar in many ways to $Fe_2S_2Cys_4$ clusters but with much higher redox potentials than found in typical $Fe_2S_2Cys_4$ proteins.[1−3] It has been generally assumed that this redox potential shift reflects a replacement of one or more Cys ligands by alternative ligands and there is considerable spectroscopic evidence by now that this is indeed the case.[114] We simply note here that, in future cases of unusual redox potentials, the invocation of heterogeneous ligation should not be automatic and the simpler alternative of a structurally diverse cluster environment should be seriously entertained.

Next, we have shown that a major determinant of the variations in redox potential with protein is the Coulombic interaction of the cluster with the protein, $v_{Q\mu}$. Not only does $v_{Q\mu}$ contribute directly to Δv, but its magnitude also affects $\Delta v_{Q\alpha}$ and Δv_L and therefore indirectly contributes to Δv, too. Further, we have shown that the major fraction of $\Delta v_{Q\mu}$ is the interaction with the backbone amide groups. Thus, a second important, qualitative result is that the folding of the polypeptide around the cluster is a major factor in determining its redox potential. For a given polypeptide main-chain conformation the nature of its side-chain group is of secondary importance. It follows that the protein sequence determines cluster redox potential primarily by controlling protein folding. Sequence changes which create large changes in polypeptide conformation can lead to large changes in redox potential; sequence changes which have little impact on protein conformation can be expected to cause only minor variations in redox potential.

Since Coulombic interactions decrease with increasing distance, conformational changes far from the cluster will cause smaller changes in redox potential than those in the immediate vicinity. However, it is important to stress that Coulombic interactions are long range (l/*r*) and do not diminish rapidly with distance. Thus, it is *not* the case that conformational changes *very* close to the cluster *overwhelmingly* dominate changes in $v_{Q\mu}$. This conclusion is in sharp contrast to the hypothesis that H-bonding—an extremely short range interaction—is a predominant factor in controlling cluster redox potentials.

The determination of the structure of a protein and, specifically, its backbone amide conformation, does not immediately define its redox potential; this requires calculations. We can expect, qualitatively, that the more amide groups in the environment of the cluster are oriented favorably for Coulombic interaction, the higher the potential and vice versa. At the same time, we have also shown that variations in redox potentials result from a complex interplay of factors and that there is not a simple relationship with any single variable. Understanding redox potential variations becomes increasingly complex as the variations decrease in size. Thus, it is *much* more difficult to predict—and, hence, understand—the <100 mV variations in potential among the rubredoxins than the huge (>1000 mV) variations between the HiPIPs and low-potential ferredoxins. Two things are absolutely essential for meaningful discussion of redox potential variations: atomic resolution, 3D structures, and quantitative calculations. Up till now biochemists have been obliged to attempt the interpretation of redox potential variations with very limited knowledge of structural variations and without the possibility of quantitative modeling. The increasing efficiency of protein structure determination, together with computational models of the sophistication of that described here, will permit much more reliable discussions to be undertaken in the future.

While Nature still supplies the vast majority of the [Fe-S] proteins available to biochemists, the engineering of unnatural [Fe-S] proteins—either via mutagenesis or by direct chemical synthesis—is being increasingly reported. In part, the motivation of such work is to understand natural proteins. In part, it is to create new proteins with new functionalities. The study of the structures and redox potentials of purposefully designed proteins will undoubtedly play an increasingly important role in further refining our understanding of the structure—redox potential relationship. Small proteins are more easily chemically synthesized and structurally characterized and are likely to be the predominant focus. Sequences of ~50 amino acids are already known to support $FeCys_4$, $Fe_3S_4Cys_3$, and $Fe_4S_4Cys_4$ clusters. It is very likely that a much more diverse range of both clusters and cluster environments than currently known will result from protein engineering. The payoff for the understanding of structure−property relationships in general and of redox potentials in particular should be enormous.

Acknowledgments

The first PDLD calculations on [Fe-S] proteins were carried out by Drs. G. M. Jensen and R. Langen and the studies reported here build on the foundation laid by their pioneering work. We are also grateful for Dr. Z. T. Chu for extensive technical assistance and to Professors E. T. Adman and H. M. Holden for allowing us the use of protein coordinates in advance of publication. P.J.S. and A.W. acknowledge support from NIH (GM 51972 and 40283) for this work.

References

(1) *Iron-Sulfur Proteins*, Academic Press: New York, Vols. I and II, 1973; Vol. III, Lovenberg, W., Ed., 1977; Vol. IV, Spiro, T. G., Ed., 1982.
(2) *Iron-Sulfur Proteins*, *Adv. Inorg. Chem.*; Cammack, R., Ed., Academic Press: New York, 1992; Vol. 38.
(3) Stiefel, E. I.; George, G. N. In *Bioinorganic Chemistry*; Bertini, I., Gray, H. B., Lippard, S. J.; Valentine, J. S., Eds.; University Science Books: Mill Valley, CA, 1994; Chapter 7, p 365.

(4) Cammack, R. In ref 2; p 281.
(5) Rees, D. C.; Farrelly, D. In *The Enzymes*; Sigman, D. S., Boyer, P. D., Eds., Academic Press: New York, 1990; Vol. 19, Chapter 2, p 37.
(6) Brooks, C. L.; Karplus, M.; Pettitt, B. M. *Adv. Chem. Phys.* **1988**, *71*, 1.
(7) Warshel, A. *Computer Simulation of Chemical Reactions in Enzymes and Solutions*; Wiley: New York, 1991.
(8) Langen, R.; Jensen, G. M.; Jacob, U.; Stephens, P. J.; Warshel, A. *J. Biol. Chem.* **1992**, *267*, 25625.
(9) Jensen, G. M.; Warshel, A.; Stephens, P. J. *Biochemistry* **1994**, *33*, 10911.
(10) Jollie, D. R. Unpublished results.
(11) Warshel, A.; Russell, S. T. *Q. Rev. Biophys.* **1984**, *17*, 283.
(12) Russell, S. T.; Warshel, A. *J. Mol. Biol.* **1985**, *389*, 185.
(13) There have been quantum mechanical calculations on [Fe-S] clusters; see, for example: Noodleman, L.; Case, D. A. In ref 2; p 425.
(14) Warshel, A.; Åqvist, J. *Annu. Rev. Biophys. Biophys. Chem.* **1991**, *20*, 267.
(15) Churg, A. K.; Warshel, A. *Biochemistry* **1986**, *25*, 1675.
(16) Warshel, A.; Creighton, S. In *Computer Simulation of Biomolecular Systems*; van Gunsteren, W. F., Weiner, P. K., Eds.; ESCOM: Leiden, 1989; p 120.
(17) Parson, W. W.; Chu, Z. T.; Warshel, A. *Biochim. Biophys. Acta* **1990**, *1017*, 251.
(18) Lee, F. S.; Chu, Z. T.; Warshel, A. *J. Comput. Chem.* **1993**, *14*, 161.
(19) Langen, R.; Brayer, G. D.; Berghuis, A. M.; Mclendon, G.; Sherman, F.; Warshel, A. *J. Mol. Biol.* **1992**, *224*, 589.
(20) Adman, E. T.; Peters-Libeu, C.; Turley, S. *Abstract of Papers*, 205th National Meeting of the American Chemical Society, Denver, CO, Spring 1993; American Chemical Society: Washington, DC, 1993; Abstract 430, Inorganic Division.
(21) It might appear that changes in Δv would more correctly be compared to changes in the redox enthalpy, ΔH, rather than the redox free energy, ΔG. For reasons discussed at length elsewhere (ref 14) this is not the case.
(22) Van Vleck, J. H. *The Theory of Electric And Magnetic Susceptibilities*; Oxford University Press: Oxford, 1932; Chapter 2.
(23) For a comparison of results obtained using eq 9 to the predictions of a more rigorous all-atom solvent model, See: King, G.; Warshel, A. *J. Chem. Phys.* **1989**, *91*, 3647.
(24) Noodleman, L.; Norman, J. G.; Osborne, J. H.; Aizman, A.; Case, D. A. *J. Am. Chem. Soc.* **1985**, *107*, 3418.
(25) Previously reported calculations[8,9] used a 2 Å inner grid; a 1 Å grid is now preferred.
(26) Jensen, L. H. In *Iron-Sulfur Proteins*; Lovenberg, W., Ed.; Academic Press: New York, 1973; Vol. II, Chapter 4, p 163.
(27) Carter, C. W. In *Iron-Sulfur Proteins*; Lovenberg, W., Ed.; Academic Press: New York, 1977; Vol. III, Chapter 6, p 157.
(28) Watenpaugh, K. D.; Sieker, L. C.; Jensen, L. H. *J. Mol. Biol.* **1980**, *138*, 615.
(29) Stenkamp, R. E.; Sieker, L. C.; Jensen, L. H. *Proteins: Struct. Funct. Genet.* **1990**, *8*, 352.
(30) Frey, M.; Sieker, L.; Payan, F.; Haser, R.; Bruschi, M.; Pepe, G.; LeGall, J. *J. Mol. Biol.* **1987**, *197*, 525.
(31) Dauter, Z.; Sieker, L. C.; Wilson, K. S. *Acta Crystallogr., Sect. B* **1992**, *48*, 42.
(32) Day, M. W.; Hsu, B. T.; Joshua-Tor, L.; Park, J. B.; Zhou, Z. H.; Adams, M. W. W.; Rees, D. C. *Protein Sci.* **1992**, *1*, 1494.
(33) Nordlund, P. Personal communication, 1995.
(34) Archer, M.; Huber, R.; Tavares, P.; Moura, I.; Moura, J. J. G.; Carrondo, M. A.; Sieker, L. C.; LeGall, J.; Romao, M. J. *J. Mol. Biol.* **1995**, *251*, 690.
(35) Jacobson, B. L.; Chae, Y. K.; Markley, J. L.; Rayment, I.; Holden, H. M. *Biochemistry* **1993**, *32*, 6788.
(36) Holden, H. M. Personal Communication, 1996. For the earlier 2.5 Å structure (PDB File 1FXA), see: Rypniewski, W. R.; Breiter, D. R.; Benning, M. M.; Wesenberg, G.; Oh, B. H.; Markley, J. L.; Rayment, I.; Holden, H. M. *Biochemistry* **1991**, *30*, 4126.
(37) Tsukihara, T.; Fukuyama, K.; Mizushima, M.; Harioka, T.; Kusunoki, M.; Katsube, Y.; Hase, T.; Matsubara, H. *J. Mol. Biol.* **1990**, *216*, 399.
(38) Ikemizu, S.; Bando, M.; Sato, T.; Morimoto, Y.; Tsukihara, T.; Fukuyama, K. *Acta Crystallogr. Sect. D* **1994**, *50*, 167.
(39) Fukuyama, K.; Ueki, N.; Nakamura, H.; Tsukihara, T.; Matsubara, H. *J. Biochem. (Tokyo)* **1995**, *117*, 1017.
(40) Sussman, J. L.; Shoham, M.; Harel, M. *Computer Assisted Modeling of Receptor-Ligand Interactions*; Rein, R., Golombek, A., Eds.; 1989; p 171.
(41) Pochapsky, T. C.; Ye, X. M.; Ratnaswamy, G.; Lyons, T. A. *Biochemistry* **1994**, *33*, 6424.
(42) Correll, C. C.; Batie, C. J.; Ballou, D. P.; Ludwig, M. L. *Science* **1992**, *258*, 1604.
(43) Romao, M. J.; Archer, M.; Moura, I.; Moura, J. J. G.; LeGall, J.; Engh, R.; Schneider, M.; Hof, P.; Huber, R. *Science* **1995**, *270*, 1170.
(44) Merritt, E. A.; Stout, G. H.; Turley, S.; Sieker, L. C.; Jensen, L. H.; Orme-Johnson, W. H. *Acta Crystallogr. Sect D.* **1993**, *49*, 272.
(45) Stout, C. D. *J. Mol. Biol.* **1989**, *205*, 545.
(46) Stout, C. D. *J. Biol. Chem.* **1993**, *268*, 25920.
(47) Kissinger, C. R.; Sieker, L. C.; Adman, E. T.; Jensen, L. H. *J. Mol. Biol.* **1991**, *219*, 693.
(48) Robbins, A. H.; Stout, C. D. *Proteins: Struct. Funct. Genet.* **1989**, *5*, 289.
(49) Volbeda, A.; Charon, M. H.; Piras, C.; Hatchikian, E. C.; Frey, M.; Fontecilla-Camps, J. C. *Nature* **1995**, *373*, 580.
(50) Carter, C. W.; Kraut, J.; Freer, S. T.; Xuong, N. H.; Alden, R. A.; Bartsch, R. G. *J. Biol. Chem.* **1974**, *249*, 4212.
(51) Holden, H. M. Personal Communication, 1996. For the earlier 2.5 Å structure (PDB File 2HIP) see: Breiter, D. R.; Meyer, T. E.; Rayment, I.; Holden, H. M. *J. Biol. Chem.* **1991**, *266*, 18660.
(52) Benning, M. M.; Mayer, T. E.; Rayment, I.; Holden, H. M. *Biochemistry* **1994**, *33*, 2476.
(53) Rayment, I.; Wesenberg, G.; Meyer, T. E.; Cusanovich, M. A.; Holden, H. M. *J. Mol. Biol.* **1992**, *228*, 672.
(54) Banci, L.; Bertini, I.; Dikiy, A.; Kastrau, D. H. W.; Luchinat, C.; Sompornpisut, P. *Biochemistry* **1995**, *34*, 206.
(55) Banci, L.; Bertini, I.; Eltis, L. D.; Felli, I. C.; Kastrau, D. H. W.; Luchinat, C.; Piccioli, M.; Pierattelli, R.; Smith, M. *Eur. J. Biochem.* **1994**, *225*, 715.
(56) Fukuyama, K.; Matsubara, H.; Tsukihara, T.; Katsube, Y. *J. Mol. Biol.* **1989**, *210*, 383.
(57) Duee, E.; Fanchon, E.; Vicat, J.; Sieker, L.; C. Meyer, J.; Moulis, J.-M. *J. Mol. Biol.* **1994**, *243*, 683.
(58) Tranqui, D.; Jesior, J. C. *Acta Crystallogr. Sect. D* **1995**, *51*, 155.
(59) Sery, A.; Housset, D.; Serre, L.; Bonicel, J.; Hatchikian, C.; Frey, M.; Roth, M. *Biochemistry* **1994**, *33*, 15408.
(60) Adman, E. T. Personal communication, 1994. See also: Backes, G.; Mino, Y.; Loehr, T. M.; Meyer, T. E.; Cusanovich, M. A.; Sweeney, W. V.; Adman, E. T.; Sanders-Loehr, J. *J. Am. Chem. Soc.* **1991**, *113*, 2055.
(61) Georgiadis, M. M.; Komiya, H.; Chakrabarti, P.; Woo, D.; Kornuc, J. J.; Rees, D. C. *Science* **1992**, *257*, 1653.
(62) Rees, D. C. Private communication, 1993.
(63) Chan, M. K.; Mukund, S.; Kletzin, A.; Adams, M. W. W.; Rees, D. C. *Science* **1995**, *267*, 1463.
(64) Lim, L. W.; Shamala, N.; Mathews, F. S.; Steenkamp, D. J.; Hamlin, R.; Xuong, N. H. *J. Biol. Chem.* **1986**, *261*, 15140.
(65) Smith, J. L.; Zaluzec, E. J.; Wery, J.-P.; Niu, L.; Switzer, R. L.; Zalkin, H.; Satow, Y. *Science* **1994**, *264*, 1427.
(66) Bertini, I.; Donaire, A.; Feinberg, B. A.; Luchinat, C.; Piccioli, M.; Yuan, H. P. *Eur. J. Biochem.* **1995**, *232*, 192.
(67) Shen, B.; Jollie, D. R.; Stout, C. D.; Diller, T. C.; Armstrong, F. A.; Gorst, C. M.; LaMar, G. N.; Stephens, P. J.; Burgess, B. K. *J. Biol. Chem.*, **1994**, *269*, 8564.
(68) Shen, B.; Martin, L. L.; Butt, J. N.; Armstrong, F. A.; Stout, C. D.; Jensen, G. M.; Stephens, P. J.; LaMar, G. N.; Gorst, C. M.; Burgess, B. K. *J. Biol. Chem.* **1993**, *268*, 25928.
(69) Shen, B. Jollie, D. R.; Diller, T. C.; Stout, C. D.; Stephens, P. J.; Burgess, B. K. *Proc. Natl. Acad. Sci. USA* **1995**, *92*, 10064.
(70) Martin, A. E.; Burgess, B. K.; Stout, C. D.; Cash, V. L.; Dean, D. R.; Jensen, G. M.; Stephens, P. J. *Proc. Natl. Acad. Sci. USA* **1990**, *87*, 598.
(71) Soman, J.; Iismaa, S.; Stout, C. D. *J. Biol. Chem.* **1991**, *266*, 21558.
(72) Kuo, C. F.; McRee, D. E.; Fisher, C. L.; O'Handley, S.; Cunningham, R. P.; Tainer, J. A. *Science* **1992**, *258*, 434.
(73) Robbins, A. H.; Stout, C. D. *Proc. Natl. Acad. Sci. USA* **1989**, *86*, 3639.
(74) Lovenberg, W.; Sobel, B. E. *Proc. Natl. Acad. Sci. USA* **1965**, *54*, 193.
(75) Hormel, S.; Walsh, K. A.; Prickril, B. C.; Titani, K.; LeGall, J.; Sieker, L. C. *FEBS Lett.* **1986**, *201*, 147.
(76) Moura, I.; Moura, J. J. G.; Santos, M. H.; Xavier, A. V.; LeGall, J. *FEBS Lett.* **1979**, *107*, 419.
(77) Shimizu, F.; Ogata, M.; Wakabayashi, S.; Matsubara, H. *Biochimie* **1989**, *71*, 1171.
(78) Adams, M. W. W. In ref 2; p 341.
(79) Pierik, A. J.; Wolbert, R. B. G.; Portier, G. L.; Verhagen, M. F. J. M.; Hagen, W. R. *Eur. J. Biochem.* **1993**, *212*, 237.
(80) Moura, I.; Xavier, A. V.; Cammack, R.; Bruschi, M.; LeGall, J. *Biochim. Biophys. Acta* **1978**, *533*, 156.
(81) Böhme, H.; Schrautemeier, B. *Biochim. Biophys. Acta* **1987**, *891*, 1.
(82) Cammack, R.; Rao, K. K.; Bargeron, C. P.; Hutson, K. G.; Andrew, P. W.; Rogers, L. J. *Biochem. J.* **1977**, *168*, 205.
(83) Sligar, S. G.; Gunsalus, A. C. *Proc. Natl. Acad. Sci. USA* **1976**, *73*, 1078.
(84) Barata, B. A. S.; Liang, J.; Moura, I.; LeGall, J.; Moura, J. J. G.; Huynh, B. H. *Eur. J. Biochem.* **1992**, *204*, 773.
(85) Iismaa, S. E.; Vazquez, A. E.; Jensen, G. M.; Stephens, P. J.; Butt, J. N.; Armstrong, F. A.; Burgess, B. K. *J. Biol. Chem.* **1991**, *266*, 21563.
(86) Cammack, R.; Rao, K. K.; Hall, D. O.; Moura, J. G.; Xavier, A. V.; Bruschi, M.; LeGall, J.; Deville, A.; Gayda, J. P. *Biochim. Biophys. Acta* **1977**, *490*, 311.

(87) Emptage, M. H.; Dreyer, J. L.; Kennedy, M. C.; Beinert, H. *J. Biol. Chem*. **1983**, *258*, 11106.
(88) Teixeria, M.; Moura, I.; Xavier, A. V.; DerVartanian, D. V.; LeGall, J.; Peck, Jr., H. D.; Huynh, B. H.; Moura, J. J. G. *Eur. J. Biochem*. **1983**, *130*, 481.
(89) Mizrahi, I. A.; Meyer, T. E.; Cusanovich, M. A. *Biochemistry* **1980**, *19*, 4727.
(90) Eltis, L. D.; Iwagami, S. G.; Smith, M. *Protein Eng*. **1994**, *7*, 1145.
(91) Heering, H. A.; Bulsink, Y. B. M.; Hagen, W. R.; Meyer, T. E. *Biochemistry* **1995**, *34*, 14675.
(92) Przysiecki, C. T.; Meyer, T. E.; Cusanovich, M. A. *Biochemistry* **1985**, *24*, 2542.
(93) Mullinger, R. N.; Cammack, R.; Rao, K. K.; Hall, D. O.; Dickson, D. P. E.; Johnson, C. E.; Rush, J. D.; Simpopoulos, A. *Biochem. J*. **1975**, *151*, 55.
(94) Stombaugh, N. A.; Sundquist, J. E.; Burris, R. H.; Orme-Johnson, W. H. *Biochemistry* **1976**, *15*, 2633.
(95) Hatchikian, E. C.; Cammack, R.; Patil, D. S.; Robinson, A. E.; Richards, A. J. M.; George, S.; Thomson, A. J. *Biochim. Biophys. Acta* **1984**, *784*, 40.
(96) Watt, G. D.; Wang, Z. C.; Knotts, R. R. *Biochemistry* **1986**, *25*, 8156.
(97) Pace, C. P.; Stankovich, M. T. *Arch. Biochem. Biophys*. **1991**, *287*, 97.
(98) Onate, Y. A.; Vollmer, S. J.; Switzer, R. L.; Johnson, M. K. *J. Biol. Chem*. **1989**, *164*, 18386.
(99) Teixeria, M.; Moura, I.; Xavier, A. V.; Moura, J. J. G.; LeGall, J.; DerVartanian, D. V.; Peck, H. D., Jr.; Huynh, B. H. *J. Biol. Chem*. **1989**, *164*, 16435.
(100) Smith, E. T.; Feinberg, B. A. *J. Biol. Chem*. **1990**, *265*, 14371.
(101) Hase, T.; Wada, K.; Matsubara, H. *J. Biochem*. **1977**, *82*, 267; 277.
(102) Moura, J. J. G.; Xavier, A. V.; Cammack, R.; Hall, D. O.; Bruschi, M.; LeGall, J. *Biochem. J*. **1978**, *173*, 419.
(103) Fukuyama, D.; Nagahara, Y.; Tsukihara, T.; Katsube, Y. *J. Mol. Biol*. **1988**, *199*, 183.
(104) Fu, W.; O'Handley, S.; Cunningham, R. P.; Johnson, M. K. *J. Biol. Chem*. **1992**, *267*, 16135.
(105) Dugad, L. B.; LaMar, G. N.; Banci, L.; Bertini, I. *Biochemistry* **1990**, *29*, 2263.
(106) Stephens, P. J.; Jensen, G. M.; Devlin, F. J.; Morgan, T. V.; Stout, C. D.; Martin, A. E.; Burgess, B. K. *Biochemistry* **1991**, *30*, 3200.
(107) Macedo, A. L.; Palma, P. N.; Moura, I.; LeGall, J.; Wray, V.; Moura, J. J. G. *Magn. Res. Chem*. **1993**, *31*, 559.
(108) Trimethyl amine dehydrogenase being the exception to this rule. Redox potentials have been reported from +100 to −40 mV. See ref 97.
(109) In the case of *Cv*HiPIP, X-ray irradiation of crystals of reduced protein caused oxidation.[27] It is not known whether this phenomenon occurs in other HiPIPs.
(110) Adman, E. T.; Watenpaugh, K. D.; Jensen, L. H. *Proc. Natl. Acad. Sci. USA* **1975**, *72*, 4854.
(111) Redox potentials were also reported for the $Fe_3S_4Cys_3$ cluster of the *Av*FdI mutants. Detectable change was observed only in the case of D15N.[68]
(112) Cunningham, R. P.; Asahara, H.; Bank, J. F.; Scholes, C. P.; Salerno, J. C.; Surerus, K.; Münck, E.; McKracken, J.; Peisach, J.; Emptage, M. H. *Biochemistry* **1989**, *28*, 4450.
(113) Luchinat, C.; Capozzi, F.; Borsari, M.; Battistuzzi, G.; Sula, M. *Biochem. Biophys. Res. Commun*. **1994**, *203*, 436.
(114) Gurbiel, R. J.; Batie, C. J.; Sivaraja, M.; True, A. E.; Fee, J. A.; Hoffman, B. M.; Ballou, D. P. *Biochemistry* **1989**, *28*, 4861.

CR950045W